Title: **A computationally fast and accurate procedure for the identification of the Chaboche isotropic-kinematic hardening model parameters based on strain-controlled cycles and asymptotic ratcheting rate**

Authors: **C. Santus, T. Grossi, L. Romanelli, M. Pedranz, M. Benedetti.**

DOI Link: https://doi.org/10.1016/j.ijplas.2022.103503

A computationally fast and accurate procedure for the identification of the Chaboche isotropic-kinematic hardening model parameters based on strain-controlled cycles and asymptotic ratcheting rate

C. Santus[a,*], T. Grossi[a], L. Romanelli[a], M. Pedranz[b], M. Benedetti[b]

[a]*Department of Civil and Industrial Engineering – DICI, University of Pisa, Italy.*
[b]*Department of Industrial Engineering – DII, University of Trento, Italy.*

Abstract

The Chaboche isotropic-kinematic hardening (CIKH) model provides a versatile and realistic description of the material stress-strain behavior under generic multiaxial cyclic loadings. However, identifying the backstress parameters is challenging, and can be formulated as an optimization problem using different approaches. Instead of a computationally expensive pointwise search, in this paper the global properties of the cyclic curves are fitted to the experimental data. The conditions introduced are the hysteresis areas, peak stress values and tangent moduli at the extreme points, however the framework can be easily adapted to other target quantities. One linear and two non-linear backstress components of the kinematic hardening model are introduced, although the analytical equations developed can be used to refine the model further, with more components. Two stabilized cycles are required to identify the main kinematic parameters. New analytical expressions for asymptotic ratcheting rates in uniaxial tests are developed and then used to tune the dynamics of the slightly non-linear (hence, slowest) backstress component. After obtaining the kinematic parameters, isotropic hardening laws can also be identified, by considering the evolution of the extreme points of the strain-controlled cycles before stabilization. Practical demonstrations of the procedure are provided by experimental tests carried out on a 7075-T6 aluminum alloy, 42CrMo4+QT steel, and a high-silicon ferritic ductile cast iron. An accurate reproduction of the material behavior is achieved, at a negligible computational cost.

Keywords: Stress relaxation (A); Constitutive behavior (B); Elastic-plastic material (B); Mechanical testing (C); Numerical algorithms (C).

Highlights

- A procedure is proposed for identifying Chaboche model parameters.
- The main global properties of the stabilized cycles and the ratcheting are imposed.
- The isotropic component parameters are easily found after the kinematic ones.
- Analytical expressions for the asymptotic ratcheting rate are found and implemented.
- Applications of the procedure on different metals are provided with validations.

*Corresponding author: Ciro Santus
Ph. +39 (0)50 2218007
Email address: ciro.santus@unipi.it (C. Santus)

Graphical Abstract

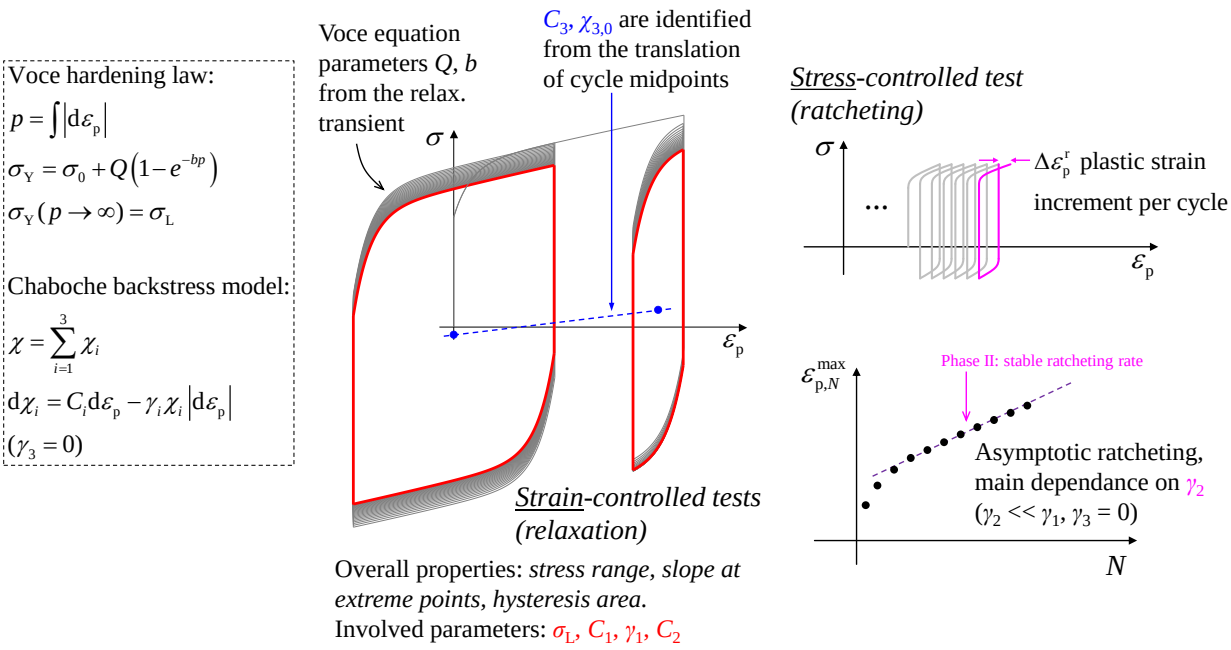

Overall properties: *stress range, slope at extreme points, hysteresis area.*
Involved parameters: σ_L, C_1, γ_1, C_2

Nomenclature

CIKH	Chaboche isotropic-kinematic hardening
σ	stress component for a uniaxial stress state
E	Young's modulus
ν	Poinsson's ratio
ε	strain along the direction of σ
ε_e	elastic component of the strain ε
ε_p	plastic component of the strain ε
χ	total uniaxial backstress, along the direction of σ
χ_i	i-th uniaxial backstress component ($i = 1, \ldots, n$)
n	number of backstress components (in the application of the present study study: $n = 3$)
χ_k	possible linear backstress component
σ_0	initial elastic limit or initial yield surface size
σ_Y	generic elastic limit depending on the isotropic hardening
σ_L	elastic limit after isotropic hardening saturation
Q, b	Parameters of Voce's law, multiplicative and exponential terms, respectively
C_i, γ_i	parameters of the i-th backstress component, linear and rate terms, respectively
C_j, γ_j	parameters of a slightly non-linear backstress component ($\gamma_j \ll \gamma_i \ \forall i$), if present
C_k, γ_k	parameters of the linear backstress component ($\gamma_k = 0$), if present
λ	root of a characteristic polynomial, for stability testing
$\chi_i^{max}, \chi_i^{min}$	i-th backstress maximum and minimum asymptotes, respectively
$\chi_{i,0}$	initial value of the i-th backstress component at the beginning of each ramp
$\chi_{k,0}$	initial value of the linear backstress component
$\varepsilon_{i,0}$	initial i-th plastic strain value at the beginning of each ramp

$\varepsilon_{\mathrm{p}}^{\min}, \varepsilon_{\mathrm{p}}^{\max}$	Minimum and maximum plastic strain of a plastic strain controlled cycle
$\Delta\varepsilon_{\mathrm{p}}$	Plastic strain amplitude of a cycle
$\chi_{i,N}^{\min}, \chi_{i,N}^{\max}$	Minimum and maximum backstress values of N-th cycle
N	number of cycle
$\chi_{i,\mathrm{stab}}^{\min}, \chi_{i,\mathrm{stab}}^{\max}$	Minimum and maximum backstress values of the stabilized cycle
$\chi_{k,\mathrm{stab}}^{\min}, \chi_{k,\mathrm{stab}}^{\max}$	Minimum and maximum stabilized values of the linear backstress component
$\sigma_N^{\min}, \sigma_N^{\max}$	Minimum and maximum stress of N-th cycle
$\sigma_{\mathrm{stab}}^{\min}, \sigma_{\mathrm{stab}}^{\max}$	Minimum and maximum stress of a stabilized cycle
σ_{m}	mean stress of a stabilized cycle, or that of the ratcheting loading
$\Delta\sigma$	stress full range of a stabilized cycle, or that of the ratcheting loading
A	Area of the hysteresis loop of the stabilized cycle
$\sigma_{\min}, \sigma_{\max}$	Minimum and maximum stresses of the ratcheting test
$\Delta\varepsilon_{\mathrm{p},N}^{+}, \Delta\varepsilon_{\mathrm{p},N}^{-}$	plastic strain amplitude, at cycle N, during ascending and decreasing ramp, respectively
$\varepsilon_{\mathrm{p},N}^{\max}, \varepsilon_{\mathrm{p},N}^{\min}$	maximum and minimum plastic strain during a ratcheting cycle, at the generic cycle N
$\Delta\varepsilon_{\mathrm{p},N}^{\mathrm{a}}, \Delta\varepsilon_{\mathrm{p},N}^{\mathrm{s}}$	ratcheting plastic strain amplitude and shift, respectively, at the generic cycle N
$\Delta\varepsilon_{\mathrm{p}}^{\mathrm{a}}, \Delta\varepsilon_{\mathrm{p}}^{\mathrm{s}}$	ratcheting plastic strain amplitude and shift, respectively, stable values
$\Delta\varepsilon_{\mathrm{p},N}^{\mathrm{r}}$	ratcheting plastic strain rate per cycle, at the generic cycle N
$\Delta\varepsilon_{\mathrm{p}}^{\mathrm{r}}$	ratcheting plastic strain rate per cycle, stable value
$\varepsilon_{\mathrm{p,stab}}^{\max}, \varepsilon_{\mathrm{p,stab}}^{\min}$	maximum and minimum plastic strain of the stabilized ratcheting cycle, if present
$\varepsilon_{\mathrm{p,stab}}^{\mathrm{m}}$	mean value between $\varepsilon_{\mathrm{p,stab}}^{\max}$ and $\varepsilon_{\mathrm{p,stab}}^{\min}$
$\varepsilon_{\mathrm{p}}^{\mathrm{m}}$	mean value of the plastic strain of a stabilized cycle
$\varepsilon_{\mathrm{p,I}}^{\mathrm{m}}, \varepsilon_{\mathrm{p,II}}^{\mathrm{m}}$	mean value of the plastic strain of the stabilized cycles I and II
$\sigma_{\mathrm{m,I}}, \sigma_{\mathrm{m,II}}$	mean stress of the stabilized cycles I and II
$\Delta\sigma_{\mathrm{I}}, \Delta\sigma_{\mathrm{II}}$	stress full range of the stabilized cycles I and II
$\Delta\varepsilon_{\mathrm{p,I}}, \Delta\varepsilon_{\mathrm{p,II}}$	Plastic strain amplitude of the stabilized cycles I and II
$\sigma_{\mathrm{stab,I}}^{\max}, \sigma_{\mathrm{stab,II}}^{\max}$	Maximum stress of the stabilized cycles I and II
$a_{\mathrm{I}}, a_{\mathrm{II}}, b_{\mathrm{I}}, b_{\mathrm{II}}$	dummy variables for the determination of C_1 and C_2
$\sigma_{\mathrm{L,I}}, \sigma_{\mathrm{L,II}}$	identified elastic limits of the stabilized cycles I and II
$A_{\mathrm{I}}, A_{\mathrm{II}}$	hysteresis area of the stabilized cycles I and II
Σ	relative peak stress error
$\Lambda_{\mathrm{I}}, \Lambda_{\mathrm{II}}$	relative hysteresis area error for the stabilized cycles I and II
$\Psi(\gamma_1)$	dimensionless error function for the determination of the parameter γ_1
R	stress ratio $\sigma^{\min}/\sigma^{\max}$, in ratcheting tests
R_ε	strain ratio $\varepsilon_{\mathrm{p}}^{\min}/\varepsilon_{\mathrm{p}}^{\max}$, in relaxation tests
ε_{d}	transverse or diametrical experimental strain
$P_{\max}$	maximum load applied to specimen under the experimental ratcheting test
B	coefficient of the geometric progression followed by $\Delta\varepsilon_{\mathrm{p},N}^{\mathrm{s}}$
ω	common ratio of the geometric progression followed by $\Delta\varepsilon_{\mathrm{p},N}^{\mathrm{s}}$
G	alternative representation of ω as $\exp(-G\Delta\varepsilon_{\mathrm{p}}^{\mathrm{a}})$
χ_i^{m}	average of maximum and minimum i-th backstress values of a cycle
$\chi_{i,N}^{\mathrm{m}}$	average of maximum and minimum i-th backstress values during the N-th cycle
$\chi_{i,N}^{\mathrm{m,forced}}$	forced response of the linear difference equation which describes the evolution of $\chi_{i,N}^{\mathrm{m}}$
$\chi_{i,N}^{\mathrm{m,free}}$	free response of the linear difference equation which describes the evolution of $\chi_{i,N}^{\mathrm{m}}$
θ_i	coefficient of the free response of $\chi_{i,N}^{\mathrm{m}}$, to be determined with boundary constraints

1. Introduction

An accurate description of the elastic-plastic behavior of metals is usually recommended for the reliable prediction of the mechanical responses of components and structures beyond the elastic limit. There are many industrial applications involving plasticity, such as the contact mechanics over the elastic limit (Mohammadpour and Chakherlou, 2016), and the fatigue loading of mechanical components (Paul et al., 2014; Paul, 2020). During load cycling, the local stress and strain histories can be significantly affected by the plasticity, especially at notches (Bertini et al., 2017). However, the simple linear elastic model is often used, mainly because of the lack of information on the constitutive behavior of the material.

One of the most common constitutive rules used to model the plasticity of metals is the Chaboche kinematic hardening model. This model was initially introduced by Chaboche (Chaboche, 1986), after developing the Armstrong and Frederick (A-F) model (Armstrong and Frederick, 1966) by proposing the superposition of multiple backstress components with different properties. The Chaboche model can be efficiently combined with an isotropic hardening rule. The exponential formula proposed by Voce (Voce, 1948) is usually considered, as in recent studies on the modeling of constitutive material behavior (Broggiato et al., 2008; Zakavi et al., 2010; Nath et al., 2019). By combining Chaboche kinematic hardening and Voce isotropic hardening, a complete model is obtained, which is usually referred to as Chaboche (or Chaboche-Lemaitre) combined isotropic-kinematic hardening (CIKH). Despite several modifications and new approaches were provided, such as (Chaboche, 2008), this hardening model remains the benchmark, for both the kinematic component alone and the combined isotropic-kinematic model. It is indeed implemented in commercial finite element software packages such as Ansys (see the theory reference manual, section 4.2 (Ansys, 2013)).

The Chaboche kinematic hardening model has been used in many applications to model different loading conditions such as indentation (Song and Komvopoulos, 2014), residual stresses (Zobec and Klemenc, 2021), and the simulation of sheet metal springback (Wagoner et al., 2013), etc. The elastic-plastic predictions of this model have also been extended to fatigue analysis, when the elastic limit exceeds a volume of a certain size around a notch, as shown for example by Branco et al. (2018), Benedetti et al. (2020) and Zhao et al. (2021). In these latter studies, the purely elastic and total (elastic-plastic) strain energy densities were identified, which were investigated as fatigue estimators. Another interesting contribution of the kinematic model, within the fatigue framework, is the prediction of the mean stress relaxation during fatigue loading (Bertini et al., 2017; Chaboche et al., 2012; Agius et al., 2017).

Different modifications of the Chaboche model have been proposed in the last few decades and also more recently. An elaborate distortion of the yield surface was considered by Rokhgireh et al. (Rokhgireh et al., 2017), to better predict uniaxial and multiaxial ratcheting tests. Non-proportional cyclic strain hardening was modelled by Xue et al. (Xue et al., 2021) to better reproduce the multiaxial loading. Another modification of the original Chaboche model is the proposal of a hardening rule with four backstress components and one with a threshold (referred to as C-H4T (Chaboche and Jung, 1997; Han et al., 2020)) in order to obtain more realistic biaxial ratcheting modeling. Lee et al. (2014), Ramezansefat and Shahbeyk (2015) and Kang (2008) also addressed the need for a modification of the Chaboche kinematic hardening rule to obtain a more accurate representation of ratcheting behavior. The original Chaboche model has also been expanded and adapted to include strain memory effects (Zhou et al., 2018), thermal softening (Zhu et al., 2016), secondary hardening (Bemfica and Castro, 2021), creep deformation (Zhang and Xuan, 2017) and dynamic strain aging (Cao et al., 2021). The constitutive models obtained are phenomenological: they describe macroscopic behavior through mathematical equations whose parameters are, however, not trivially related to a measurable quantity. On the other hand, the

development of crystal plasticity models which connect the macroscopic behavior with the underlying physical micro-scale mechanisms have attracted increasing interest (Bandyopadhyay et al., 2021; Li et al., 2022a).

Uniaxial stress- or strain-controlled cyclic tests are frequently performed to characterize the material response, and different behaviors can be observed: purely elastic, elastic shakedown, plastic shakedown, or ratcheting, often with a steady strain increment (Koo et al., 2019; Paul, 2019). However, when a small portion of the material undergoes cyclic plasticity and that volume is surrounded by the bulk of material remaining below the elastic limit (as in notched components), the resulting loading at the notch root can be interpreted as a mixed stress- and strain-controlled loading. More precisely, as described in Fig. 1, three regions can be distinguished around a notch under fatigue loading beyond the elastic limit, as noted by Paul and Tarafder (2013). The outer region (far from the stress concentration) remains elastic and provides a deformation constraint for the inner region. The intermediate region experiences an elastic shakedown, while the material around the notch tip undergoes a plastic shakedown. In this latter (and most critical) region, when the external load imposes an asymmetric cycle, a stress relaxation is initially observed, which in principle is beneficial for fatigue under tensile stresses. This stress relaxation near the notch was modeled and also experimentally observed by Shekarian and Varvani-Farahani (2019, 2021). After some relaxation, this initial trend usually evolves into a ratcheting behavior until complete stabilization, as shown in Fig. 1 and discussed by Paul (2016); Zhao et al. (2021). Ratcheting and stabilized behavior are thus arguably the most critical aspects of material modeling in the fatigue of notched components.

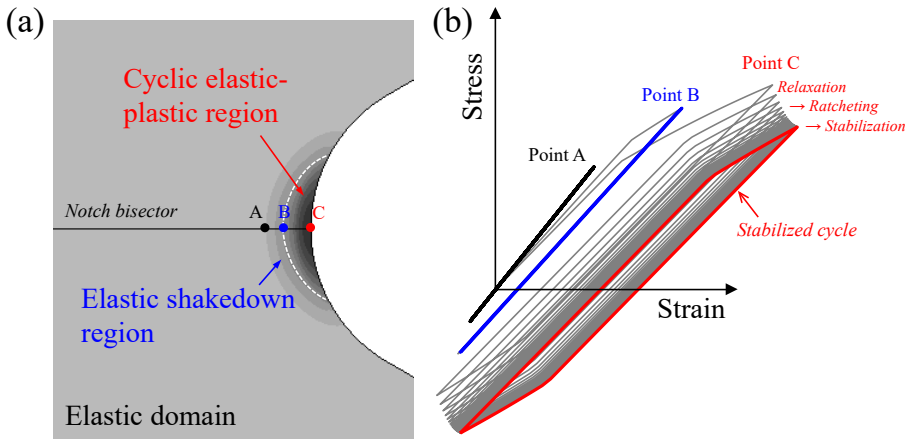

Figure 1: Elastic and elastic-plastic shakedown at the notch root while the outer volume remains elastic.

Ratcheting can induce either ductile or brittle (low-cycle) fatigue failure (Kang et al., 2008, 2009), which can evolve as an elastic-plastic shakedown or continue until specimen failure. When the latter occurs, the ratcheting evolution can be divided into primary, secondary and tertiary zones (or stages), as in Paul et al. (2010); Paul (2012); Zhang et al. (2020). In the secondary zone, an approximately constant ratcheting rate (intended as the strain increase per cycle) is observed. This is a well-known experimental result, as shown by Hassan and Kyriakides (1992); Kreethi et al. (2017); Zhang et al. (2020), and the modeling of this phenomenon is among the main targets of various proposals regarding hardening rules. A detailed review of both experimental observations and constitutive modeling aspects of ratcheting can be found in (Kang, 2008).

Using either the original Chaboche model or one of the modified models, evaluating the material parameters and in particular the backstress coefficients is challenging. Different approaches to this identification problem are available in the literature. An interesting approach was proposed by Liu et al. (2019) referring to stabilized (and symmetric) cycles for the identification process, while tuning the value of the smallest γ_i to meet the ratcheting strain prediction. Lee et al. (2014) also proposed the combination of uniaxial strain-controlled cycling loadings

at different strain amplitudes, in combination with additional ratcheting tests to verify and fine-tune the material model. As detailed later, this paper also follows a similar approach. Hai et al. (2021) used strain-controlled tests, and both the isotropic and kinematic rules were modified with respect to the original Chaboche model, also including the evolution of the elastic modulus depending on the (cumulative) plastic strain. The identification of parameters is often performed using ratcheting tests (both uniaxial and biaxial, the latter obtained as axial load plus torsion), as in Agius et al. (2017); Abdel-Karim (2010); Ding et al. (2012); Bari and Hassan (2000); Hamidinejad and Varvani-Farahani (2015).

When the material model is particularly refined and the kinematic hardening parameters are only a subset of a larger parameter set, a numerical optimization is usually used (Zhu et al., 2016; Cao et al., 2021; Burgold et al., 2020; Egner et al., 2020; Esmaeili et al., 2017; Hwang et al., 2020; Okorokov et al., 2019; Song and Komvopoulos, 2014; Cheong et al., 2018; Xie et al., 2019; Xu et al., 2016, 2022), in order to minimize the deviation between experimental and simulated stress histories. In these cases, as observed by Cao et al. (2021) and Okorokov et al. (2019), a strategy that decouples the effects of some parameters and identifies them separately is fundamental. For example, stabilized hysteresis loops often identify kinematic hardening parameters alone (Xie et al., 2019). Xu et al. (2016) verified their model (which included Chaboche kinematic hardening) by also comparing simulated and experimental hysteresis areas. As the complexity of constitutive models has increased, machine learning approaches have been used to obtain data-driven material models (Abueidda et al., 2021; Li et al., 2022b).

Several examples of parameter identifications using genetic algorithms have been presented (Nath et al., 2019; Mahmoudi et al., 2011; Badnava et al., 2012; Nath et al., 2021). Mahmoudi et al. (2011) proposed a multi objective optimization with two fitness functions, using a genetic algorithm search for the Chaboche kinematic hardening parameters. One of these fitness functions was aimed at accurately reproducing the hysteresis cycle, while the other was used to model ratcheting behavior, and the results were similar to the C-H4T model, also for multiaxial ratcheting. Another example of multi-objective optimization was proposed by Sinaie et al. (2014) and the target consisted in a pointwise modeling of experimental load histories, until a Pareto frontier was reached. Wójcik and Skrzat (2020, 2021) implemented a fuzzy logic approach for the correction and optimization of the Chaboche parameters. A particle swarm optimization algorithm was implemented by Moslemi et al. (2020) and then used to model uniaxial and biaxial ratcheting tests of AISI 316L stainless steel.

A more direct approach can be obtained by using backstress components to model the hardening behavior at different length scales. Instead of running a complex optimization task, the cyclic curves can be considered in segments, and the most effective coefficients of each of them can be obtained in a stepwise manner (Arora et al., 2021; Das et al., 2020; Yuenyong and Uthaisangsuk, 2020; Yang et al., 2020).

Fu et al. (2016) determined the model parameters with the virtual fields method, in combination with a full-field deformation measurement, and different numbers of backstress components (from one to three) were considered, just to fit the initial loading cycles. Nath et al. (2019) argued that ratcheting tests can be accurately simulated only if isotropic hardening is also included, and that the absence of isotropic hardening in cyclically stable materials should be carefully evaluated on a case-by-case basis.

This paper considers the original Chaboche kinematic hardening model, and an identification procedure is presented along with experimental data on 7075-T6 aluminum, 42CrMo4+QT steel, and a high-silicon ferritic ductile cast iron. After obtaining the kinematic parameters of these materials, the models are also refined with the introduction of an isotropic hardening law such as Voce's equation, thus creating a full CIKH model. As clarified in Section 2, since the procedure is initially aimed at reproducing quantities that *do not depend* on the

specific isotropic hardening behavior, the choice of the that model does not affect the identification process. Hence, the isotropic model parameters can be identified later when the kinematic parameters are available. For this reason, more complex isotropic hardening laws can be included.

The classical CIKH model has some limitations. For example, it does not consider non-proportional hardening and strain memory effects. However, for many engineering and building materials, it represents a solid compromise between accuracy and complexity, requiring only 6 kinematic (in the 3-backstress setup) and 2 isotropic parameters, in addition to the material elastic properties.

The proposed identification process only requires uniaxial tests to determine the whole set of CIKH parameters, thereby keeping experimental requirements to a minimum. Given that the Chaboche model has some limitations and its backstress components are not directly related to physical quantities, in principle there are no *correct* parameters, thus the identification should be performed for a specific target, as discussed for example by Djimli et al. (2010). In other words, the *right* parameters are those that *work best* at predicting the material behavior in some loading conditions of practical interest. More specifically, the main target of the present procedure is to accurately reproduce the stabilized cycles obtained under strain-controlled conditions. This target is of particular interest for the fatigue of notched components, in which a portion of the volume at the notch undergoes cyclic plasticity, while the surrounding material remains elastic (as in Fig. 1). However, since a short ratcheting phase is often present in this case, the aim is also to achieve a realistic reproduction of uniaxial ratcheting. Proportional loadings are very common when notched components are tested under fatigue, as loads are usually scaled over time. In addition, tensile and bending tests induce a moderate multiaxiality at the notch tip, so this configuration is similar to proportional uniaxial loading.

As shown in the following of the paper, ratcheting behavior has a substantial dependence on parameters that have a negligible effect on stabilized cycles, therefore accurate identification cannot be based only on the latter. Although the classical CIKH model is often believed to be unsatisfactory in reproducing even uniaxial ratcheting tests, accurate results are possible if the calibration process takes advantage of at least one stress-controlled test. Parameter identification is implemented by imposing *global* properties of stabilized uniaxial cycles and not by minimizing a pointwise discrepancy function. The global properties considered are the hysteresis area of the stabilized loop, the peak stress values, and the tangent modulus at the extreme points. These properties are the main interesting ones in the fatigue assessment, while the transitional evolution of the initial cycles leading to stabilization is considered less critical, since it is usually short in comparison. This approach is not limited to fatigue modeling, since it can be used to decouple kinematic hardening parameters from an unknown isotropic law and therefore to determine them independently. In order to let stabilized cycles have non-zero mean stresses, a linear backstress component (with $\gamma_i = 0$) is imposed, and only two other (non-linear) components are considered, although the addition of more components is addressed. Analytical expressions are provided for the conditions to be matched, and the whole identification is reduced to the numerical minimization of a single-variable function, leading to an easy determination of the parameters.

Hassan et al. (2008) showed that, by tuning the smallest γ_i, the asymptotic ratcheting rate can be matched without affecting the reproduction of strain-controlled cycles. This paper similarly shows that the identification of the smallest γ_i is mainly governed by the approximately constant ratcheting rate in the secondary phase, and analytical relations between those two quantities are presented. To the best of our knowledge, to date no analytical expression for the stabilized ratcheting rate has been published.

An additional factor plays an important role in the identification of constitutive laws from experimental data. Since the problem is highly non-linear, numerical algorithms are used, whose complexity often increases

with that of the constitutive model requiring identification. The existence of a single set of globally optimal parameters can seldom be taken for granted, which gives the identification process a significant degree of arbitrariness. For example, the starting point of the optimization algorithm, the termination criteria for numerical iterations, and the optimization algorithm itself affect the results obtained. Even the simple non-linear regression of three A-F exponential laws on a stabilized cycle is often seriously ill-conditioned. In contrast, the proposed procedure is *deterministic*. Once the global properties of stabilized cycles are available, the corresponding model parameters are unambiguously determined. In fact, the only numerical computation required is the global minimization of a single-variable (and quite smooth) function ranging on a limited domain, which can be performed deterministically in negligible time. Then, although some tools to fine-tune the identification process are provided (as detailed in Section 3), numerical issues are avoided.

2. Formulation of the cyclic loading modelling

2.1. Chaboche kinematic hardening model

In uniaxial stress conditions, σ is the single non-zero principal stress for a uniaxial loading, such as in a simple plain specimen under pure tension, and the strain along that direction is ε, which is the sum of the elastic and plastic strains:

$$\varepsilon = \varepsilon_{\mathrm{e}} + \varepsilon_{\mathrm{p}} \tag{1}$$

A kinematic hardening model is described by the following constitutive equation:

$$|\sigma - \chi| \leq \sigma_{\mathrm{Y}} \tag{2}$$

where σ_{Y} is the material elastic limit. In uniaxial conditions σ is a scalar value, and the choice of a specific yield surface (e.g., Von Mises or Tresca) does not change the yield behavior, as it is completely defined by the parameters χ and σ_{Y}. For this reason, when plastic flow is active, Eq. (2) can be rewritten as:

$$\sigma = \chi \pm \sigma_{\mathrm{Y}} \tag{3}$$

where the sign depends on whether the load is towards tension or compression.

According to the Chaboche model (Chaboche, 1986), the (total) backstress can be considered as the sum of multiple backstress components:

$$\chi = \sum_{i=1}^{n} \chi_i \tag{4}$$

and each of them evolves according to the well-known differential equation:

$$\mathrm{d}\chi_i = C_i \mathrm{d}\varepsilon_{\mathrm{p}} - \gamma_i \chi_i |\mathrm{d}\varepsilon_{\mathrm{p}}| \tag{5}$$

Eq. (2) controls the shift of the yield surface through a scalar backstress χ, which defines the current centre of the surface. Since a purely kinematic hardening is described, the radius of the yield surface is kept constant and it is the saturated value of elastic limit σ_{Y}, which is referred to as σ_{L} (limit) in the present paper. Note that in other works the symbol σ_0 is frequently used, while here the *limit* value σ_{L} will be distinguished from the *initial* value σ_0. However, the isotropic hardening component will be addressed later.

Eq. (4) states that the backstress χ is decomposed as a sum of i additive components χ_i, where i ranges from 1 to n. Each backstress component behaves according to an Armstrong-Frederick (A-F) hardening rule (Armstrong and Frederick, 1966), found in Eq. (5) in its differential form and determined by two positive parameters C_i and γ_i which can be defined, respectively, as the the linear and the rate coefficients.

Due to the simultaneous presence of terms $\mathrm{d}\varepsilon_\mathrm{p}$ and $|\mathrm{d}\varepsilon_\mathrm{p}|$, Eq. (5) does not have a general solution in closed form. However, it can be split into two cases, obtaining two linear differential equations:

$$\begin{aligned} \frac{\mathrm{d}\chi_i}{\mathrm{d}\varepsilon_\mathrm{p}} &= C_i - \gamma_i \chi_i \quad \text{if } \mathrm{d}\varepsilon_\mathrm{p} > 0 \\ \frac{\mathrm{d}\chi_i}{\mathrm{d}\varepsilon_\mathrm{p}} &= C_i + \gamma_i \chi_i \quad \text{if } \mathrm{d}\varepsilon_\mathrm{p} < 0 \end{aligned} \tag{6}$$

Thus, for a given sign of $\mathrm{d}\varepsilon_\mathrm{p}$ (namely, an algebraically increasing or decreasing load), Eq. (5) becomes a first-order linear differential equation. Eqs. (6) are usually solved as Cauchy initial-value problems: for a known initial value of χ_i, its evolution with respect to ε_p is simulated. Depending on the sign of $\mathrm{d}\varepsilon_\mathrm{p}$, the first or the second equation is active and controls the behavior of χ_i.

If $\gamma_i > 0$ (*strictly* positive), the equilibrium points of the system of Eqs. (6) can be easily obtained by setting $\mathrm{d}\chi_i/\mathrm{d}\varepsilon_\mathrm{p} = 0$ and are denoted with $\chi_i^{\max}$ and $\chi_i^{\min}$:

$$\begin{aligned} \chi_i^{\max} &= \frac{C_i}{\gamma_i} \quad \text{ascending ramp} \\ \chi_i^{\min} &= -\frac{C_i}{\gamma_i} \quad \text{descending ramp} \end{aligned} \tag{7}$$

Both Eqs. (6) share their characteristic polynomial, which is $\lambda + \gamma_i = 0$, so they have the same negative characteristic root $\lambda = -\gamma_i$ and their behavior is asymptotically stable. Thus, all solutions monotonically tend to one of their equilibrium points $\chi_i^{\max}$ or $\chi_i^{\max}$ (depending on the sign of $\mathrm{d}\varepsilon_\mathrm{p}$), regardless of the initial value of χ_i. The well-known general solution of Eqs. (6) can be obtained through direct integration:

$$\begin{aligned} \chi_i(\varepsilon_\mathrm{p}) &= \frac{C_i}{\gamma_i} + \left(\chi_{i,0} - \frac{C_i}{\gamma_i}\right) \exp(-\gamma_i(\varepsilon_\mathrm{p} - \varepsilon_{\mathrm{p},0})) \quad \text{if } \varepsilon_\mathrm{p} - \varepsilon_{\mathrm{p},0} > 0 \\ \chi_i(\varepsilon_\mathrm{p}) &= -\frac{C_i}{\gamma_i} + \left(\chi_{i,0} + \frac{C_i}{\gamma_i}\right) \exp(-\gamma_i(\varepsilon_{\mathrm{p},0} - \varepsilon_\mathrm{p})) \quad \text{if } \varepsilon_\mathrm{p} - \varepsilon_{\mathrm{p},0} < 0 \end{aligned} \tag{8}$$

where $\varepsilon_{\mathrm{p},0}$ is the initial value of ε_p and $\chi_{i,0}$ is the corresponding initial value of χ_i, namely: $\chi_{i,0} = \chi_i(\varepsilon_{\mathrm{p},0})$. As predicted, the solutions of Eqs. (8) asymptotically tend to the equilibrium values reported in Eqs. (7): C_i/γ_i for $\varepsilon_\mathrm{p} \gg \varepsilon_{\mathrm{p},0}$ and $-C_i/\gamma_i$ for $\varepsilon_\mathrm{p} \ll \varepsilon_{\mathrm{p},0}$, respectively.

If there is a backstress component, denoted with a specific index k, having $\gamma_k = 0$, Eq. (5) becomes $\mathrm{d}\chi_k = C_k \mathrm{d}\varepsilon_\mathrm{p}$, so the relationship between χ_k and ε_p is linear and does not depend on the sign of $\mathrm{d}\varepsilon_\mathrm{p}$:

$$\chi_k(\varepsilon_\mathrm{p}) = \chi_{k,0} + C_k(\varepsilon_\mathrm{p} - \varepsilon_{\mathrm{p},0}) \tag{9}$$

For this reason, χ_k is commonly referred to as the *linear* backstress component, while the other components

χ_i, with $\gamma_i > 0$, are the *non-linear* ones, as they model non-linear trends in the constitutive behavior. Note that having more than one linear component would be redundant, since from Eq. (9) they would be equivalent to a single linear component obtained by summing their $\chi_{k,0}$ and C_k parameters.

When a material undergoes a cyclic loading which generates a hysteresis loop, backstress components χ_i alternatively switch between the two Eqs. (6), depending on whether the specimen is in the ascending or descending ramp. Since every ramp has a finite amplitude, the two equilibrium points $\chi_i^{\max}$ and $\chi_i^{\min}$ are never reached. The behavior defined by Eqs. (8) is shown in Fig. 2, where the linear term is also reported, according to Eq. (9).

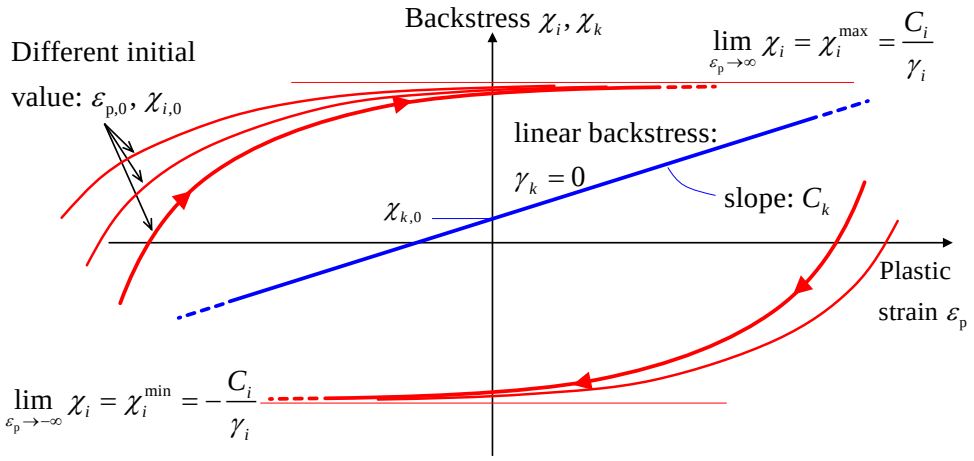

Figure 2: Asymptotes of a non-linear backstress along the two ramps and simple relationship of the linear backstress.

In formal terms, the Chaboche model takes a set of material parameters and a set of test parameters as input and yields a stress-strain history as an output. On the other hand, a parameter identification procedure takes experimental data as input and yields a set of material parameters. In the framework of inverse problem theory (see the textbook of Hansen (2010) for an engineering reference), these two processes would be called, respectively, a direct problem and its inverse problem.

An implicit assumption of every parameter identification strategy is that the experimental data are always a valid output of the model whose parameters are to be identified. Equivalently, the direct and the inverse problem share their mathematical model, yet with partially reversed relations between input and output variables. That assumption is clearly ideal, seldom attainable in practice, and it introduces errors in the predictions of experiments, which often cannot be phenomenologically distinguished from errors in the identification process. This error source is commonly referred to as *model error* in inverse problem theory. For example, a material stress-strain history might be affected by some degree of creep or strain-memory effects, which could not be modeled by Eqs. (2), (4) and (5). In addition, the number n of backstress components controls the degrees of freedom of the Chaboche model. In absence of physical hints on how many components shall be included, n should be chosen as a tradeoff between model complexity and predictive performances. This choice will be addressed in Section 3.3.

Since a general analytical solution of the direct problem is not available (mainly due to Eq. (5)), an analytical inversion of the mathematical relations between the Chaboche material parameters and their corresponding stress-strain histories is unfeasible. Thus, a different approach is pursued here. In the following sections, the *direct problem* is studied further, in order to obtain analytical relations between a set of model parameters (assumed to be known) and some appropriately defined quantities of practical interest which can be measured

in an experimental test. Eventually, the inversion can be carried out on those quantities and not on the entire stress-strain histories, with clear computational advantages.

2.2. Uniaxial cyclical test in plastic strain control

Although uncommon in the experimental practice, an effective test would be a relaxation test under *plastic* strain control (instead of total strain).

The plastic strain ranges from $\varepsilon_{\mathrm{p}}^{\min}$ to $\varepsilon_{\mathrm{p}}^{\max}$, so the cycle amplitude is $\Delta\varepsilon_{\mathrm{p}} = \varepsilon_{\mathrm{p}}^{\max} - \varepsilon_{\mathrm{p}}^{\min}$. $\chi_{i,N}^{\max}$ and $\chi_{i,N}^{\min}$ are defined as the values of backstress component i at the end of the ascending and descending ramp of cycle N. Strictly positive γ_i's are assumed for now, and every cycle is conventionally assumed to start with an ascending ramp. Applying the first of Eqs. (8) to $\chi_{i,N}^{\max}$, a closed-form expression for $\chi_{i,N}^{\min}$ can be found:

$$\chi_{i,N}^{\min} = -\frac{C_i}{\gamma_i} + \left(\chi_{i,N}^{\max} + \frac{C_i}{\gamma_i}\right)\exp(-\gamma_i\Delta\varepsilon_{\mathrm{p}}) \tag{10}$$

The subsequent ascending ramp can be computed, to find $\chi_{i,N+1}^{\max}$:

$$\chi_{i,N+1}^{\max} = \frac{C_i}{\gamma_i} + \left(\chi_{i,N}^{\min} - \frac{C_i}{\gamma_i}\right)\exp(-\gamma_i\Delta\varepsilon_{\mathrm{p}}) \tag{11}$$

Eq. (10) can be substituted in Eq. (11), obtaining the following expression, which relates the maximum backstress at cycle $N+1$ to the one at cycle N:

$$\chi_{i,N+1}^{\max} = \frac{C_i}{\gamma_i}(1-\exp(-\gamma_i\Delta\varepsilon_{\mathrm{p}}))^2 + \chi_{i,N}^{\max}\exp(-2\gamma_i\Delta\varepsilon_{\mathrm{p}}) \tag{12}$$

Being C_i, γ_i and $\Delta\varepsilon_{\mathrm{p}}$ constants, Eq. (12) is a first-order linear difference equation, whose characteristic root is $\lambda = \exp(-2\gamma_i\Delta\varepsilon_{\mathrm{p}})$; since $|\lambda| < 1$, it is asymptotically stable. In agreement with Chaboche (1986), the stabilized value $\chi_{i,\mathrm{stab}}^{\max}$ can be found by setting $\chi_{i,N}^{\max} = \chi_{i,N+1}^{\max} = \chi_{i,\mathrm{stab}}^{\max}$ in Eq. (12). The following well-known relation is obtained:

$$\chi_{i,\mathrm{stab}}^{\max} = \frac{C_i}{\gamma_i}\frac{1-\exp(-\gamma_i\Delta\varepsilon_{\mathrm{p}})}{1+\exp(-\gamma_i\Delta\varepsilon_{\mathrm{p}})} = \frac{C_i}{\gamma_i}\tanh\left(\frac{\gamma_i\Delta\varepsilon_{\mathrm{p}}}{2}\right) \tag{13}$$

The same procedure can be analogously applied to $\chi_{i,N}^{\min}$, obtaining:

$$\chi_{i,\mathrm{stab}}^{\min} = -\frac{C_i}{\gamma_i}\tanh\left(\frac{\gamma_i\Delta\varepsilon_{\mathrm{p}}}{2}\right) \tag{14}$$

Due to asymptotic stability of Eq. (12), $\chi_{i,N}^{\max}$ and $\chi_{i,N}^{\min}$ tend to the stabilized values $\chi_{i,\mathrm{stab}}^{\max}$ and $\chi_{i,\mathrm{stab}}^{\min}$, respectively, regardless of any initial value $\chi_{i,0}$. Moreover, $\chi_{i,\mathrm{stab}}^{\min} = -\chi_{i,\mathrm{stab}}^{\max}$, meaning that each backstress reaches stability as a symmetrically alternating component, with null mean value. The peak stress values at the end of each loading ramp can be easily found by combining Eqs. (3) and (4):

$$\begin{aligned}\sigma_{\mathrm{stab}}^{\max} &= \sum_{i=1}^{n}\chi_{i,\mathrm{stab}}^{\max} + \sigma_{\mathrm{L}}\\ \sigma_{\mathrm{stab}}^{\min} &= \sum_{i=1}^{n}\chi_{i,\mathrm{stab}}^{\min} - \sigma_{\mathrm{L}}\end{aligned} \tag{15}$$

The stabilization behavior of the extreme values of σ is schematically described in Fig. 3(a). As described in

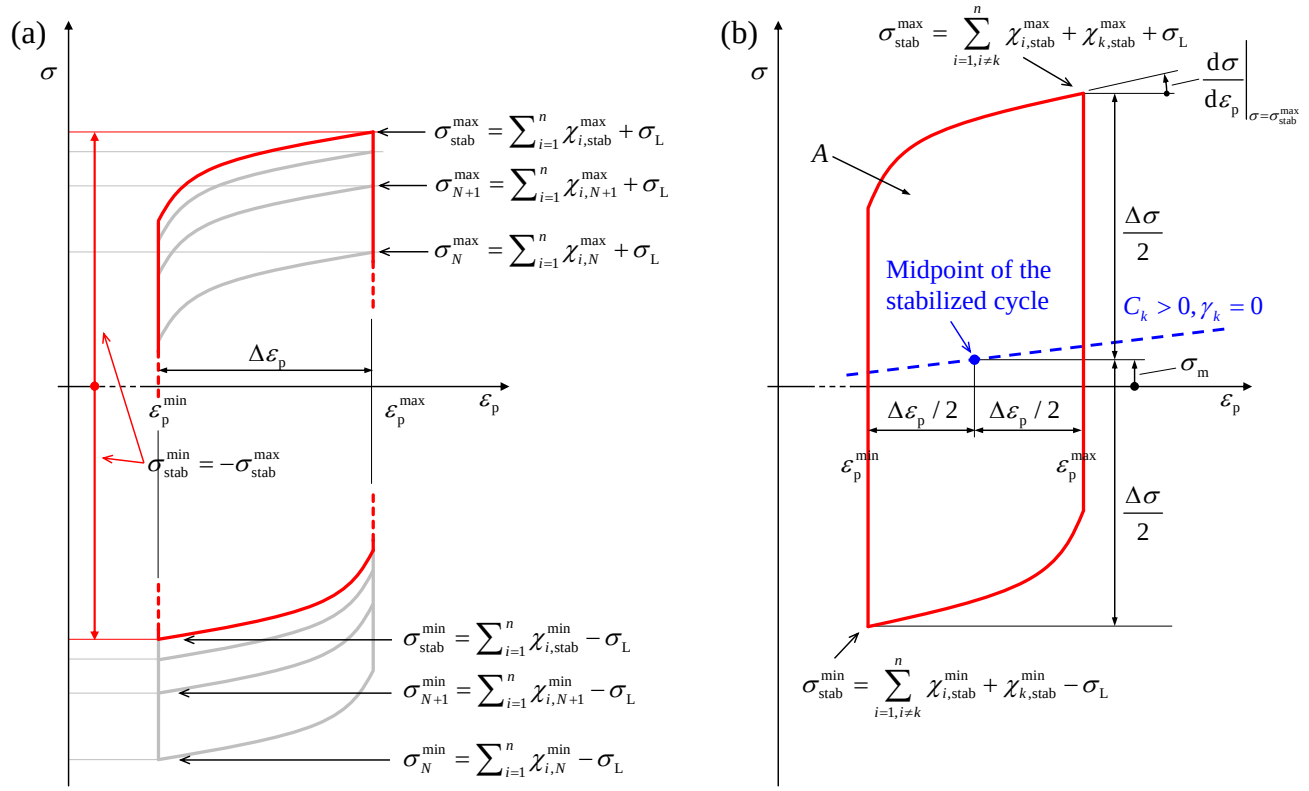

Figure 3: Definition of cycle variables at the extreme points of cycles in plastic strain control. Stabilized cycles are in red. (a) When only non-linear components are present, the stabilized cycle is symmetric regardless of any initial asymmetry. (b) Asymmetry is controlled by the parameters of the linear backstress component.

the figure, the mean stress of the stabilized cycle is zero. Equivalently, $\sigma_{\text{stab}}^{\min} = -\sigma_{\text{stab}}^{\max}$. However, this significant result is only valid if all the backstress components are non-linear ($\gamma_i > 0$). If a linear backstress is introduced (which will be denoted here with the special index k), the additional two terms below need to be considered:

$$\begin{aligned} \chi_{k,\text{stab}}^{\max} &= \chi_{k,0} + C_k \varepsilon_{\text{p}}^{\max} \\ \chi_{k,\text{stab}}^{\min} &= \chi_{k,0} + C_k \varepsilon_{\text{p}}^{\min} \end{aligned} \tag{16}$$

The evolution of this backstress component is simply a straight line in the σ vs. ε_{p} plane, therefore these two extreme values are already the stabilized ones. The mean stress of the cycle when including the linear backstress is:

$$\sigma_{\text{m}} = \frac{\sigma_{\text{stab}}^{\min} + \sigma_{\text{stab}}^{\max}}{2} = \chi_{k,0} + C_k \frac{\varepsilon_{\text{p}}^{\min} + \varepsilon_{\text{p}}^{\max}}{2} \tag{17}$$

and its effect is shown in Fig. 3(b). The stress full range is:

$$\Delta\sigma = \sigma_{\text{stab}}^{\max} - \sigma_{\text{stab}}^{\min} = \sum_{i=1}^{n} \left(\chi_{i,\text{stab}}^{\max} - \chi_{i,\text{stab}}^{\min} \right) + 2\sigma_{\text{L}} = \sum_{i=1,\ i\neq k}^{n} 2\frac{C_i}{\gamma_i} \tanh\left(\frac{\gamma_i \Delta\varepsilon_{\text{p}}}{2} \right) + C_k \Delta\varepsilon_{\text{p}} + 2\sigma_{\text{L}} \tag{18}$$

The equations that have been developed up to this point are well-known in the literature on the Chaboche model, but they provide common ground for the new analytical relations that will be provided in this manuscript from now on.

In many practical cases, the area of the stabilized hysteresis cycle is needed as an input for other predictive

models (e.g., for low-cycle fatigue). As shown in Appendix A.1, it can be expressed as follows:

$$A = \oint \sigma \, \mathrm{d}\varepsilon_\mathrm{p} = 2\sigma_\mathrm{L}\Delta\varepsilon_\mathrm{p} + 2\sum_{i=1,\ i\neq k}^{n}\left(\frac{C_i}{\gamma_i}\Delta\varepsilon_\mathrm{p} - 2\frac{C_i}{\gamma_i^2}\tanh\left(\frac{\gamma_i\Delta\varepsilon_\mathrm{p}}{2}\right)\right) \tag{19}$$

Chaboche himself (Chaboche, 1986) suggests that a linear backstress component should be used to model the approximately linear last part of a single large loading ramp, where the tangent modulus is much smaller than Young's modulus. Therefore, the relation between the ramp slope just before load inversion and the model parameters is of particular interest. The evaluation of this slope can be found in Eq. (20) (details are in Appendix A.2):

$$\left.\frac{\mathrm{d}\sigma}{\mathrm{d}\varepsilon_\mathrm{p}}\right|_{\sigma=\sigma_\mathrm{stab}^\mathrm{max}} = \sum_{i=1\ i\neq k}^{n} C_i\left(1-\tanh\left(\frac{\gamma_i\Delta\varepsilon_\mathrm{p}}{2}\right)\right) + C_k \tag{20}$$

and the same value can be obtained for the end of the descending ramp, at $\sigma = \sigma_\mathrm{stab}^\mathrm{min}$.

A limit case arises when a non-linear backstress component has a very small rate coefficient with respect to the cycle amplitude. The special index j will be used in this particular case. More precisely, this happens when $0 < \gamma_j\Delta\varepsilon_\mathrm{p} \ll 1$. Then, the following first-order approximations hold:

$$\begin{aligned}&\exp(-\gamma_j\Delta\varepsilon_\mathrm{p}) \approx 1-\gamma_j\Delta\varepsilon_\mathrm{p}\\ &\tanh\left(\frac{\gamma_j\Delta\varepsilon_\mathrm{p}}{2}\right) \approx \frac{\gamma_j\Delta\varepsilon_\mathrm{p}}{2}\end{aligned} \tag{21}$$

Eqs. (13) and (14) become:

$$\begin{aligned}&\chi_{j,\mathrm{stab}}^\mathrm{max} = \frac{C_j\Delta\varepsilon_\mathrm{p}}{2}\\ &\chi_{j,\mathrm{stab}}^\mathrm{min} = -\frac{C_j\Delta\varepsilon_\mathrm{p}}{2}\end{aligned} \tag{22}$$

as the component j does not contribute to the hysteresis area. The area calculation reduces to:

$$A = \oint \sigma \, \mathrm{d}\varepsilon_\mathrm{p} = 2\sigma_\mathrm{L}\Delta\varepsilon_\mathrm{p} + 2\sum_{i=1,\ i\neq j,k}^{n}\left(\frac{C_i}{\gamma_i}\Delta\varepsilon_\mathrm{p} - 2\frac{C_i}{\gamma_i^2}\tanh\left(\frac{\gamma_i\Delta\varepsilon_\mathrm{p}}{2}\right)\right) \tag{23}$$

The contribution of the j-th term to the slope is just linear, like the k-th term, and Eq. (20) becomes:

$$\left.\frac{\mathrm{d}\sigma}{\mathrm{d}\varepsilon_\mathrm{p}}\right|_{\sigma=\sigma_\mathrm{stab}^\mathrm{max}} = \sum_{i=1\ i\neq j,k}^{n} C_i\left(1-\tanh\left(\frac{\gamma_i\Delta\varepsilon_\mathrm{p}}{2}\right)\right) + C_j + C_k \tag{24}$$

In other words, the j-th backstress behaves similarly to the k-th one, i.e. its cycle collapses to a line, and in particular the contribution to the hysteresis area is null. However, its initial value $\chi_{j,0}$ vanishes in a similar way like the other non-linear terms, though after many cycles. In fact, over many consecutive cycles the evolution of the extreme values follows Eq. (12), which has a characteristic root $\lambda = \exp(-2\gamma_j\Delta\varepsilon_\mathrm{p})$, very close but not equal to 1. This is sufficient to generate convergence to the equilibrium values of Eqs. (22). As $\gamma_j \to 0$, the convergence gets slower, but the equilibrium point is maintained. Instead, in the case $\gamma_k = 0$, the characteristic root is exactly 1, so the initial value $\chi_{k,0}$ of the backstress component χ_k remains constant after a (theoretically)

infinite number of cycles.

2.3. Uniaxial cyclic test in total strain control

A plastic strain control would require a non-trivial implementation. Therefore, a total strain control, easily achieved with an extensometer, is usually preferred. The peak stress values generally vary cycle after cycle, and so does the elastic portion of the total strain. This means that, as load cycles are carried out, the applied extreme values of plastic strain vary too. Strictly speaking, the analysis of the last section is not valid anymore, but some considerations can be done.

There are combinations of imposed total strains which lead to an elastic shakedown, a situation where the stabilized cycle lies entirely in the material elastic range and the backstress components are frozen to the last values they achieved during a plastic deformation. This happens when $\Delta\varepsilon < 2\sigma_{\mathrm{L}}/E$. Since the target is to extract the whole set of Chaboche parameters from stabilized hysteresis cycles, this case is not meaningful and will be excluded a priori. From a practical point of view, if elastic shakedown was attained during an experimental test used to calibrate the Chaboche parameters, the imposed strain amplitude would be increased. Numerical simulations generally show that for $\Delta\varepsilon > 2\sigma_{\mathrm{L}}/E$ a plastic shakedown, thus a stabilized hysteresis cycle is always reached. That is quite intuitive: the variation range of peak stress values is usually limited (especially after the first cycles), so the cycle is *almost* in plastic strain control. Even if a formal demonstration is not trivial, it is not needed in the context of a parameter identification, where experimental evidence is already given.

If a stabilized cycle is available, the specific control strategy used to enforce it is irrelevant to the material, so it may also be seen as a cycle in plastic strain control. Since the last section proved that a test under plastic strain control always yields a unique stabilized cycle, it must match the obtained experimental cycle. Eventually, the results of last section can be applied to any stabilized cycle, regardless of its control strategy, to identify a set of Chaboche model parameters.

2.4. Uniaxial cyclic test in stress control

If a cyclic loading is carried out in stress control ranging from $\sigma_{\min}$ to $\sigma_{\max}$, ratcheting may occur, and a closed cycle may never be attained. First, some variables are defined, according to Fig. 4. $\Delta\varepsilon^{+}_{\mathrm{p},N}$ and $\Delta\varepsilon^{-}_{\mathrm{p},N}$ refer to the absolute plastic strain delta during the ascending and descending ramps of cycle N. An average plastic strain amplitude of the generic cycle is defined as:

$$\Delta\varepsilon^{\mathrm{a}}_{\mathrm{p},N} = \frac{\Delta\varepsilon^{+}_{\mathrm{p},N} + \Delta\varepsilon^{-}_{\mathrm{p},N}}{2} \tag{25}$$

Since the cycle N is open in general, an average plastic strain shift per load ramp is defined:

$$\Delta\varepsilon^{\mathrm{s}}_{\mathrm{p},N} = \frac{\Delta\varepsilon^{+}_{\mathrm{p},N} - \Delta\varepsilon^{-}_{\mathrm{p},N}}{2} \tag{26}$$

Superscripts “a” and “s” in Eqs. (25) and (26) stand for “amplitude” and “shift”; respectively. The mean stress $\sigma_{\mathrm{m}} = (\sigma_{\max} + \sigma_{\min})/2$, where $\sigma_{\max}$ and $\sigma_{\min}$ are the imposed maximum and minimum stresses, is kept constant during the entire test. For now, it is assumed that a linear backstress component is absent; its effects will be discussed separately.

As done in the study of a cycle in plastic strain control, the sequences $\chi^{\max}_{i,N}$ and $\chi^{\min}_{i,N}$ are analyzed. By applying Eqs. (8), it holds:

$$\chi^{\min}_{i,N} = -\frac{C_i}{\gamma_i} + \left(\chi^{\max}_{i,N} + \frac{C_i}{\gamma_i}\right)\exp(-\gamma_i\Delta\varepsilon^{-}_{\mathrm{p},N}) \tag{27}$$

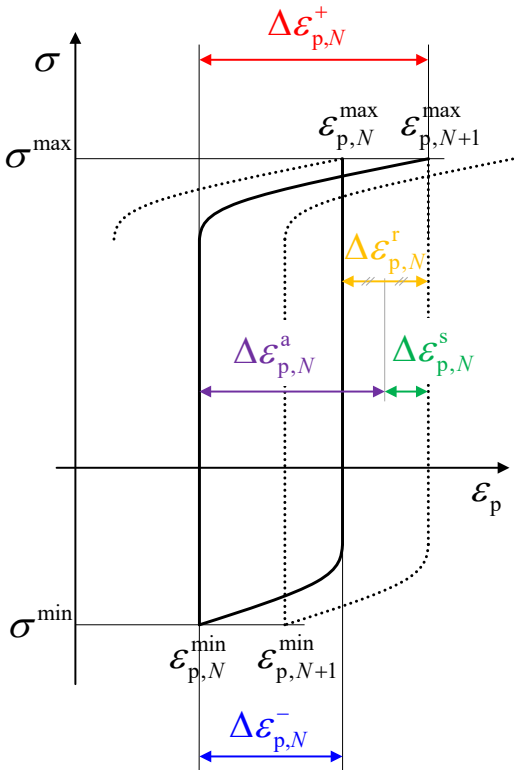

Figure 4: Stress and strain definitions of the cycle of a ratcheting test.

Then, the maximum backstress of the subsequent cycle is:

$$\chi^{\max}_{i,N+1} = \frac{C_i}{\gamma_i} + \left(\chi^{\min}_{i,N} - \frac{C_i}{\gamma_i}\right)\exp(-\gamma_i \Delta\varepsilon^{+}_{\mathrm{p},N}) \tag{28}$$

By substituting the term $\chi^{\min}_{i,N}$ of Eq. (27) into Eq. (28), and considering the definitions of Eq. (25) and Eq. (26), the maximum backstress can be reformulated as follows:

$$\chi^{\max}_{i,N+1} = 2\frac{C_i}{\gamma_i}\exp(-\gamma_i \Delta\varepsilon^{\mathrm{a}}_{\mathrm{p},N})(1-\exp(-\gamma_i \Delta\varepsilon^{\mathrm{s}}_{\mathrm{p},N})) + \frac{C_i}{\gamma_i}(1-\exp(-\gamma_i \Delta\varepsilon^{\mathrm{a}}_{\mathrm{p},N}))^2 + \chi^{\max}_{i,N}\exp(-2\gamma_i \Delta\varepsilon^{\mathrm{a}}_{\mathrm{p},N}) \tag{29}$$

Since $\Delta\varepsilon^{\mathrm{a}}_{\mathrm{p},N}$ and $\Delta\varepsilon^{\mathrm{s}}_{\mathrm{p},N}$ may vary at each cycle (as they depend on the behavior of backstress components themselves), Eq. (29) is highly non-linear and the sequence $\chi^{\max}_{i,N}$ cannot be studied analytically in the general case. However, some particular solutions of high practical interest can still be obtained. For example, it could be assumed that both $\Delta\varepsilon^{\mathrm{a}}_{\mathrm{p},N}$ and $\Delta\varepsilon^{\mathrm{s}}_{\mathrm{p},N}$ are practically at equilibrium after a certain number N of cycles. Although it may seem a very restrictive hypothesis, numerical simulations actually suggest that the behaviors of $\Delta\varepsilon^{\mathrm{a}}_{\mathrm{p},N}$ and $\Delta\varepsilon^{\mathrm{s}}_{\mathrm{p},N}$ are always asymptotically stable. Hence, the hypothesis is usually satisfied after some initial stabilization cycles. In fact, many authors report a constant ratcheting rate after an initial settling phase (Lee et al., 2014; Paul, 2012; Zhang et al., 2020; Kreethi et al., 2017; Hamidinejad and Varvani-Farahani, 2015). Under this assumption, in Eq. (29) the strain values $\Delta\varepsilon^{\mathrm{a}}_{\mathrm{p},N}$ and $\Delta\varepsilon^{\mathrm{s}}_{\mathrm{p},N}$ can be replaced with their asymptotic values $\Delta\varepsilon^{\mathrm{a}}_{\mathrm{p}}$ and $\Delta\varepsilon^{\mathrm{s}}_{\mathrm{p}}$, i.e. not depending on the cycle number N. Having assumed that $\Delta\varepsilon^{\mathrm{a}}_{\mathrm{p}}$ and $\Delta\varepsilon^{\mathrm{s}}_{\mathrm{p}}$ are constant values, a first-order linear difference equation is obtained and, again, its stability can be assessed according to its characteristic polynomial. The solution is asymptotically stable since $\lambda = \exp(-2\gamma_i \Delta\varepsilon^{\mathrm{a}}_{\mathrm{p}})$, so $|\lambda| < 1$. By setting $\chi^{\max}_{i,N+1} = \chi^{\max}_{i,N} = \chi^{\max}_{i,\mathrm{stab}}$,

after a few algebraic steps (similarly applied to the term $\chi^{\min}_{i,\mathrm{stab}}$), it holds that:

$$\begin{aligned}
\chi^{\max}_{i,\mathrm{stab}} &= \frac{C_i}{\gamma_i}(1-\exp(-\gamma_i\Delta\varepsilon^{\mathrm{s}}_{\mathrm{p}}))\,\mathrm{csch}(\gamma_i\Delta\varepsilon^{\mathrm{a}}_{\mathrm{p}}) + \frac{C_i}{\gamma_i}\tanh\left(\frac{\gamma_i\Delta\varepsilon^{\mathrm{a}}_{\mathrm{p}}}{2}\right) \\
\chi^{\min}_{i,\mathrm{stab}} &= \frac{C_i}{\gamma_i}(\exp(\gamma_i\Delta\varepsilon^{\mathrm{s}}_{\mathrm{p}})-1)\,\mathrm{csch}(\gamma_i\Delta\varepsilon^{\mathrm{a}}_{\mathrm{p}}) - \frac{C_i}{\gamma_i}\tanh\left(\frac{\gamma_i\Delta\varepsilon^{\mathrm{a}}_{\mathrm{p}}}{2}\right)
\end{aligned} \tag{30}$$

where $\mathrm{csch}(\gamma_i\Delta\varepsilon^{\mathrm{a}}_{\mathrm{p}}) = 2\exp(-\gamma_i\Delta\varepsilon^{\mathrm{a}}_{\mathrm{p}})/(1-\exp(-2\gamma_i\Delta\varepsilon^{\mathrm{a}}_{\mathrm{p}}))$, an alternative expression for the hyperbolic cosecant function.

By comparing Eqs. (30) with Eqs. (13) and (14), it follows that:

- If $\Delta\varepsilon^{\mathrm{s}}_{\mathrm{p}} > 0$ (a constant ratcheting rate towards positive strains), both $\chi^{\max}_{i,\mathrm{stab}}$ and $\chi^{\min}_{i,\mathrm{stab}}$ are algebraically higher than the values they would have attained in a cycle in strain control having equal amplitude.
- If $\Delta\varepsilon^{\mathrm{s}}_{\mathrm{p}} < 0$ (a constant ratcheting rate towards negative strains), both $\chi^{\max}_{i,\mathrm{stab}}$ and $\chi^{\min}_{i,\mathrm{stab}}$ are algebraically lower than the values they would have attained in a cycle in strain control having equal amplitude.
- If $\Delta\varepsilon^{\mathrm{s}}_{\mathrm{p}} = 0$ (a plastic shakedown occurred and the cycle is stable), both $\chi^{\max}_{i,\mathrm{stab}}$ and $\chi^{\min}_{i,\mathrm{stab}}$ match their corresponding equilibrium values in a cycle in strain control having equal amplitude.

This scenario is coherent with the experimental observations. A cycle with significantly asymmetric peak stress values is needed to develop ratcheting.

Eqs. (30) concern a single backstress component. Since peak stress values $\sigma_{\max}$ and $\sigma_{\min}$ are imposed, Eq. (3) must also be satisfied, which leads to:

$$\begin{aligned}
\sigma_{\max} &= \sum_{i=1}^{n}\chi^{\max}_{i,\mathrm{stab}} + \sigma_{\mathrm{L}} = \frac{C_i}{\gamma_i}(1-\exp(-\gamma_i\Delta\varepsilon^{\mathrm{s}}_{\mathrm{p}}))\,\mathrm{csch}(\gamma_i\Delta\varepsilon^{\mathrm{a}}_{\mathrm{p}}) + \frac{C_i}{\gamma_i}\tanh\left(\frac{\gamma_i\Delta\varepsilon^{\mathrm{a}}_{\mathrm{p}}}{2}\right) + \sigma_{\mathrm{L}} \\
\sigma_{\min} &= \sum_{i=1}^{n}\chi^{\min}_{i,\mathrm{stab}} - \sigma_{\mathrm{L}} = \frac{C_i}{\gamma_i}(\exp(\gamma_i\Delta\varepsilon^{\mathrm{s}}_{\mathrm{p}})-1)\,\mathrm{csch}(\gamma_i\Delta\varepsilon^{\mathrm{a}}_{\mathrm{p}}) - \frac{C_i}{\gamma_i}\tanh\left(\frac{\gamma_i\Delta\varepsilon^{\mathrm{a}}_{\mathrm{p}}}{2}\right) - \sigma_{\mathrm{L}}
\end{aligned} \tag{31}$$

By adding and subtracting the two equations, after a few arrangements the following relations are obtained:

$$\begin{aligned}
\sigma_{\mathrm{m}} &= \sum_{i=1}^{n}\frac{C_i}{\gamma_i}\frac{\sinh(\gamma_i\Delta\varepsilon^{\mathrm{s}}_{\mathrm{p}})}{\sinh(\gamma_i\Delta\varepsilon^{\mathrm{a}}_{\mathrm{p}})} \\
\frac{\Delta\sigma}{2} &= \sum_{i=1}^{n}\left(\frac{C_i}{\gamma_i}\frac{1-\cosh(\gamma_i\Delta\varepsilon^{\mathrm{s}}_{\mathrm{p}})}{\sinh(\gamma_i\Delta\varepsilon^{\mathrm{a}}_{\mathrm{p}})} + \frac{C_i}{\gamma_i}\tanh\left(\frac{\gamma_i\Delta\varepsilon^{\mathrm{a}}_{\mathrm{p}}}{2}\right)\right) + \sigma_{\mathrm{L}}
\end{aligned} \tag{32}$$

where, according to alternative expressions of hyperbolic functions:

$$\begin{aligned}
\sinh(\gamma_i\Delta\varepsilon^{\mathrm{s}}_{\mathrm{p}}) &= \frac{1-\exp(-2\gamma_i\Delta\varepsilon^{\mathrm{s}}_{\mathrm{p}})}{2\exp(-\gamma_i\Delta\varepsilon^{\mathrm{s}}_{\mathrm{p}})} \\
\cosh(\gamma_i\Delta\varepsilon^{\mathrm{s}}_{\mathrm{p}}) &= \frac{1+\exp(-2\gamma_i\Delta\varepsilon^{\mathrm{s}}_{\mathrm{p}})}{2\exp(-\gamma_i\Delta\varepsilon^{\mathrm{s}}_{\mathrm{p}})}
\end{aligned} \tag{33}$$

If an experimental test is available, which stabilizes on a constant strain amplitude and a constant ratcheting rate, the system of Eqs. (32) provides two conditions on the Chaboche model parameters. The two equations depend,

respectively, on the average cycle stress and on the stress amplitude. Note that if $\Delta\varepsilon_{\mathrm{p}}^{\mathrm{s}} = 0$, the first of Eqs. (32) states that σ_{m} must be null as well. Thus, in this specific condition where the linear backstress component is not considered, the Chaboche model predicts that a plastic shakedown can occur only if the input stresses are symmetric. In this case, the second of Eqs. (32) becomes:

$$\frac{\Delta\sigma}{2} = \sum_{i=1}^{n} \frac{C_i}{\gamma_i} \tanh\left(\frac{\gamma_i \Delta\varepsilon_{\mathrm{p}}^{\mathrm{a}}}{2}\right) + \sigma_{\mathrm{L}} \tag{34}$$

which is similar to Eq. (18), without a linear backstress component that still has to be included in the analysis. Analogously, the first of Eqs. (32) states that a constant ratcheting rate $\Delta\varepsilon_{\mathrm{p}}^{\mathrm{s}} > 0$ can be obtained only with $\sigma_{\mathrm{m}} > 0$, and vice versa, $\Delta\varepsilon_{\mathrm{p}}^{\mathrm{s}} < 0$ only with $\sigma_{\mathrm{m}} < 0$. Without additional hypotheses, Eqs. (32) cannot be further simplified.

The ratcheting rate per cycle can be now introduced, which is usually the quantity of interest in a ratcheting test: $\Delta\varepsilon_{\mathrm{p},N}^{\mathrm{r}} = 2\Delta\varepsilon_{\mathrm{p},N}^{\mathrm{s}}$. Its equilibrium point is denoted with $\Delta\varepsilon_{\mathrm{p}}^{\mathrm{r}}$. See Fig. 4 for a graphical representation. When $\gamma_i \Delta\varepsilon_{\mathrm{p}}^{\mathrm{s}} \ll 1$ for each backstress component $i = 1 \dots n$ (which is a fairly common case, due to the typically small strain increments per cycle), the hyperbolic functions involving $\Delta\varepsilon_{\mathrm{p}}^{\mathrm{s}}$ can be approximated with their first order Taylor polynomial, obtaining:

$$\begin{aligned} \sigma_{\mathrm{m}} &= \frac{\Delta\varepsilon_{\mathrm{p}}^{\mathrm{r}}}{2} \sum_{i=1}^{n} \frac{C_i}{\sinh(\gamma_i \Delta\varepsilon_{\mathrm{p}}^{\mathrm{a}})}) \\ \frac{\Delta\sigma}{2} &= \sum_{i=1}^{n} \frac{C_i}{\gamma_i} \tanh\left(\frac{\gamma_i \Delta\varepsilon_{\mathrm{p}}^{\mathrm{a}}}{2}\right) + \sigma_{\mathrm{L}} \end{aligned} \tag{35}$$

The second of Eqs. (35) is still equivalent to Eq. (18), so that the cycle averaged strain amplitude and its stress amplitude are related as in a stabilized cycle in strain control. The first of Eqs. (35) relates the equilibrium ratcheting rate with the average stress, the Chaboche parameters, and the cycle strain amplitude. If the stricter condition $\gamma_i \Delta\varepsilon_{\mathrm{p}}^{\mathrm{a}} \ll 1$ is also valid for each index i, Eqs. (35) can be further approximated as:

$$\begin{aligned} \sigma_{\mathrm{m}} &= \frac{\Delta\varepsilon_{\mathrm{p}}^{\mathrm{r}}}{2\Delta\varepsilon_{\mathrm{p}}^{\mathrm{a}}} \sum_{i=1}^{n} \frac{C_i}{\gamma_i} \\ \frac{\Delta\sigma}{2} &= \sum_{i=1}^{n} \frac{C_i \Delta\varepsilon_{\mathrm{p}}^{\mathrm{a}}}{2} + \sigma_{\mathrm{L}} \end{aligned} \tag{36}$$

The approximations can also be performed on individual backstress components, simplifying only some terms of Eqs. (32).

2.5. Ratcheting with linear and slightly non-linear backstress components

As discussed before, a slightly non-linear and a linear backstress components behave very similarly in a strain-controlled stabilized cycle, except for the stabilized extreme values. In the first case, they take algebraically opposite values, regardless of their starting ones. On the contrary, in the second case, they depend on the initial backstress value $\chi_{k,0}$. Since γ_i controls the convergence rate of χ_i through Eq. (12), it may be argued that the smallest non-null γ_i could be detected from the convergence rate of $\sigma_N^{\max}$ and $\sigma_N^{\min}$ to their stabilized values, but that is quite difficult on the practical side, due to: 1) experimental errors, 2) influence of the isotropic hardening on the convergence rate, 3) backstresses χ_i being not individually observable, as only their sum is physically

measured.

Chaboche himself (Chaboche, 1986) recommend that a linear backstress component should be used to model the approximately linear final part of a single large loading ramp, where the tangent modulus is much smaller than Young's modulus and almost constant. That is a widely-employed method (Zobec and Klemenc, 2021; Arora et al., 2021; Das et al., 2020). If a single ramp or stabilized cycle is available, it is a reasonable strategy. Its results may however be in contrast with the necessary conditions imposed by Eq. (17). In fact, maintaining index k for the linear component, the values of C_k and $\chi_{k,0}$ define a linear relation between the average plastic strain and the average stress. The angular coefficient C_k of that line might in general be significantly different from the tangent modulus at high strains (that is actually the case in the present work). Due to this, C_k will be identified from the linear relation between average stress and average strain, through two (or, possibly, more) experimental cycles, and not from the slope at extreme points.

Moreover, as observed by Bari and Hassan (2000), a Chaboche model should have a slightly non-linear backstress component (having a small γ_i) in order to predict the ratcheting behavior correctly, because a linear component forces a plastic shakedown to occur, which is not always true in the experimental practice. By denoting the slightly non-linear backstress component with the index j (as previously done), since γ_j usually turns out to be in the order of 1–10, it most likely satisfies $\gamma_j \Delta\varepsilon_\mathrm{p} \ll 1$ in a strain-controlled test, so that the approximations of Eqs. (21)−(24) hold. In particular, that component behaves linearly in practice, with a slope depending on its coefficient C_j (and not on γ_j). Eventually, C_j can be used to model the linear asymptote of a large loading ramp, while γ_j, whose effect on a stabilized cycle is *negligible*, is identified through the asymptotic slope of a ratcheting test and the first of Eqs. (32) or, possibly, Eqs. (35)– (36), as shown in the following. Note that, by using C_j to model the plastic tangent modulus at high strains, its value usually lies in the range 10^3–10^4, so it generally occurs that $C_j/\gamma_j \gg C_i/\gamma_i$ for all indexes $i \neq j$. If that is true and both $\gamma_i \Delta\varepsilon_\mathrm{p}^\mathrm{s} \ll 1$ and $\gamma_i \Delta\varepsilon_\mathrm{p}^\mathrm{a} \ll 1$ for all indexes i, then the first of Eqs. (36) can be approximated to a simple expression:

$$\sigma_\mathrm{m} = \frac{C_j}{\gamma_j} \frac{\Delta\varepsilon_\mathrm{p}^\mathrm{r}}{2\Delta\varepsilon_\mathrm{p}^\mathrm{a}} \tag{37}$$

which can be rewritten as:

$$\gamma_j = \frac{C_j \Delta\varepsilon_\mathrm{p}^\mathrm{r}}{2\Delta\varepsilon_\mathrm{p}^\mathrm{a} \sigma_\mathrm{m}} \tag{38}$$

If these assumptions are valid, Eq. (38) is a particularly simple and meaningful relation that allows to obtain γ_j from an experimental ratcheting test and from C_j. Since a stabilized cycle obtained in strain control is influenced by C_j but is negligibly affected by γ_j, a ratcheting test provides through Eqs. (32), (35), (36) and (38) a piece of information that is *complementary* to strain-controlled tests. Note that Eq. (38) does not imply that the ratcheting rate $\Delta\varepsilon_\mathrm{p}^\mathrm{r}$ is influenced *only* by the backstress component j alone. In fact, the equilibrium value of $\Delta\varepsilon_\mathrm{p}^\mathrm{a}$ depends on all backstress components, through the second equation in systems (32), (35) and (36). Nevertheless, if $\Delta\varepsilon_\mathrm{p}^\mathrm{a}$ and $\Delta\varepsilon_\mathrm{p}^\mathrm{r}$ are available from an experimental test, a relation like Eq. (38) provides a condition on γ_j that is *decoupled* from the strain-controlled tests.

When a linear backstress component is considered (with usual special index k), Eq. (29) becomes:

$$\chi_{k,N+1}^\mathrm{max} = \chi_{k,N}^\mathrm{max} + C_k(\Delta\varepsilon_{\mathrm{p},N}^+ - \Delta\varepsilon_{\mathrm{p},N}^-) = \chi_{k,N}^\mathrm{max} + C_k \Delta\varepsilon_\mathrm{p}^\mathrm{r} \tag{39}$$

Eq. (39) implies that a constant ratcheting rate $\Delta\varepsilon_\mathrm{p}^\mathrm{r} \neq 0$ cannot be obtained in the presence of a linear backstress component. Since the cycle is carried out in stress control, due to Eqs. (3)–(4) the backstress cannot grow

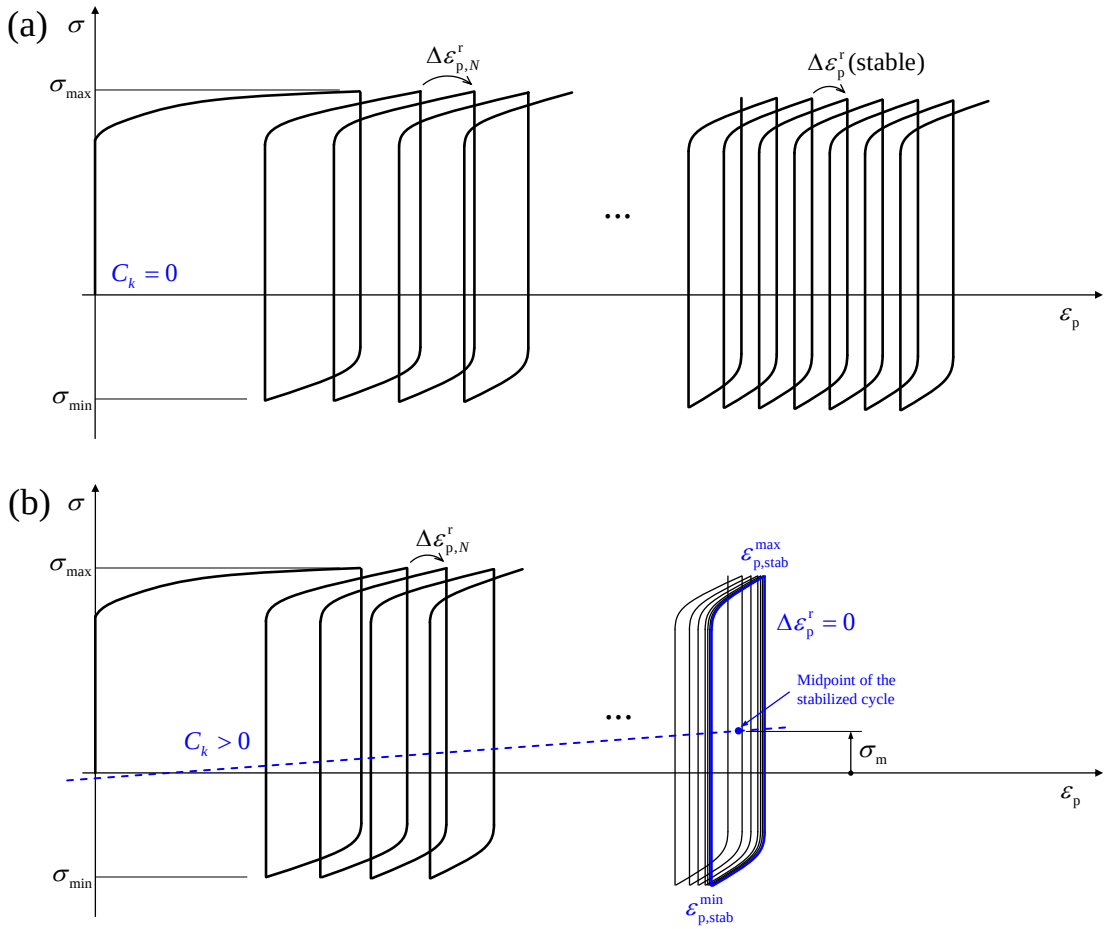

Figure 5: (a) Ratcheting rate stabilization without a linear backstress. (b) Ratcheting arrest with a linear backstress, and stabilized cycle when the linear backstress equals the mean stress.

indefinitely. Therefore, if a linear backstress component is present, the only achievable equilibrium state is a plastic shakedown ($\Delta\varepsilon^{\mathrm{r}}_{\mathrm{p}} = 0$) ranging between the plastic strains $\varepsilon^{\mathrm{min}}_{\mathrm{p,stab}}$ and $\varepsilon^{\mathrm{max}}_{\mathrm{p,stab}}$, as already stated by Bari and Hassan (2000), and numerically observed by Koo et al. (2019). In this case, all other backstress components are stabilized to algebraically opposite values $\pm C_i/\gamma_i \tanh((\gamma_i \Delta\varepsilon^{\mathrm{a}}_{\mathrm{p}})/2)$ (see Eqs. (30)), so the whole stress asymmetry is absorbed by the linear backstress component. This allows to predict the point where the ratcheting will stop, expressed in terms of average plastic strain of the stabilized cycle:

$$\begin{aligned} \sigma_{\mathrm{m}} &= \chi_{k,0} + C_k \frac{\varepsilon^{\mathrm{max}}_{\mathrm{p,stab}} + \varepsilon^{\mathrm{min}}_{\mathrm{p,stab}}}{2} \\ \varepsilon^{\mathrm{m}}_{\mathrm{p,stab}} &= \frac{\varepsilon^{\mathrm{max}}_{\mathrm{p,stab}} + \varepsilon^{\mathrm{min}}_{\mathrm{p,stab}}}{2} = \frac{\sigma_{\mathrm{m}} - \chi_{k,0}}{C_k} \end{aligned} \tag{40}$$

A pictorial representation of the effect of a linear backstress component is provided in Fig. 5. As C_k is increased, the ratcheting curve diverges from the linear asymptote corresponding to $C_k = 0$ and increases its concavity, since it must reach plastic shakedown at a lower strain (a numerical example is provided in the Discussion section). An interesting consequence is that ratcheting curve can either tend to a constant value or diverge indefinitely with a constant slope. Actually, as shown in (Paul, 2012) and in the present work, experimental ratcheting curves often show a final part where the maximum strain diverges from the linear asymptote until specimen failure. This behavior *cannot be modeled* with the original Chaboche model unless other phenomena such as damage in

the specimen are incorporated, as observed in Kang et al. (2009); Zhang et al. (2020). Interestingly, Zhu et al. (2016) showed that this behavior can also be explained by the occurrence of thermal softening effect during the ratcheting test.

Since the proposed identification process will always yield a C_k which is non-null in general, its presence should be addressed in the identification process, since, strictly speaking, it prevents the possibility of modeling a constant ratcheting rate $\Delta\varepsilon_{\mathrm{p}}^{\mathrm{s}} \neq 0$. In this case, a strategy is presented in Appendix A.3. Nevertheless, in order to successfully implement this strategy in the inverse problem, the whole convergence to plastic shakedown would be required to be experimentally available, which is often false due to specimen failure. In practice, a simpler approach may be pursued.

The effect of C_k becomes significant when the strain is high enough to generate a substantial linear backstress component, which absorbs the stress asymmetry. Since C_k is assumed to control the change in average stress following a variation in average strain, stress relaxation phenomena generally ensure that its value is moderate. For example, consider that $C_k \approx 1000$ MPa implies that shifting a strain-controlled cycle by 1% would yield a variation in the order of 10 MPa for the average stabilized stress, which is already quite a significant amount. In this case, the ratcheting curve is only marginally affected by C_k, especially in its first part. Its curvature is almost negligible, and its slope can be considered as approximately equal to the case $C_k = 0$. As a matter of fact, since a practically constant ratcheting rate is often observed in experimental tests (in the secondary phase), it can be effectively considered for the calibration of γ_j parameter, as discussed in Section 4.

2.6. Isotropic hardening

The experimental elastic limit (or, more properly, the yield surface size) also depends in general on the cumulated plastic strain, therefore showing an isotropic hardening behavior. Whenever the isotropic component is neglected, the unique value of the elastic limit is σ_0, and it is constant over time. In this analysis, σ_0 just refers to the initial yield surface size, then the elastic limit σ_{Y} can increase or decrease. For the sake of simplicity, it is assumed that σ_{Y} evolves according to Voce's (Voce, 1948) exponential equation:

$$\sigma_{\mathrm{Y}} = \sigma_0 + Q(1 - \exp(-bp)) \tag{41}$$

where Q and b are the Voce's equation parameters, respectively the multiplicative and the exponential one. The cumulated plastic strain p, for a uniaxial test is:

$$p = \int |\mathrm{d}\,\varepsilon_{\mathrm{p}}| \tag{42}$$

The integral is evaluated on the whole plastic history starting from the initial condition where the yield surface size is σ_0. After that large plastic strains have been cumulated, the elastic limit stress is obtained:

$$\sigma_{\mathrm{L}} = \sigma_0 + Q = \sigma_{\mathrm{Y}}(p \to \infty) \tag{43}$$

The variation term Q can be either positive (cyclic hardening) or negative (cyclic softening).

In the present study, since the stabilized cycles are used for calibration, the limit value σ_{L} is initially found together with the kinematic hardening parameters, while the transient during the initial cycles of the test can be considered afterwards, to find Q and b. More specifically, Eq. (3) can be applied in its general form to the

maximum stress $\sigma_N^{\max}$ of a generic cycle N:

$$\sigma_N^{\max} = \sum_{i=1}^{n} \chi_{i,N}^{\max} + \sigma_0 + Q(1 - \exp(-bp)) = \sum_{i=1}^{n} \chi_{i,N}^{\max} + \sigma_{\mathrm{L}} - Q\exp(-bp) \tag{44}$$

Eq. (44) divides the hardening process into a known kinematic term and an unknown isotropic term. Eqs. (43) and (44) can be rearranged into:

$$\sigma_{\mathrm{Y}} - \sigma_{\mathrm{L}} = \sum_{i=1}^{n} \chi_{i,N}^{\max} - \sigma_N^{\max} - \sigma_{\mathrm{L}} = -Q\exp(-bp) \tag{45}$$

Since p is available from experimental data, Q and b can be obtained with a least-squares fit of Eq. (45) over the extreme points of available test cycles, as shown in Section 4.

As long as the material shows a Masing behavior (Jiang and Zhang, 2008), Eqs. (44)-(45) can be fitted with any isotropic law which is dependent on the cumulated plastic strain. When strain memory effects are present (Zhang and Jiang, 2008), another approach shall be adopted. For example, several values of σ_{L} corresponding to different maximum plastic strains could be obtained from Eqs. (56), allowing the identification of a strain memory surface.

3. Proposed identification procedure

Starting from the analysis of the *direct* problem, a procedure for the inverse problem of parameters identification can be now proposed. Its only mathematical challenge lies in the minimization of a single-variable function on a given interval, which can be obtained almost instantaneously on a common PC.

The identification of Chaboche parameters is ultimately done to predict the material behavior in different and potentially more complex cases, with respect to the experimental tests. To the authors' best knowledge, Chaboche parameters are never involved as direct inputs to other material models and are not (currently) linked to a measurable quantity. In formal terms, errors are to be measured in stress-strain space and not in parameters space. This is of particular importance, because there are some combinations of very different Chaboche parameters which yield almost indistinguishable material behaviors. For example, two sufficiently small γ_i's, potentially orders of magnitude far from each other, both lead to an approximately linear behavior on a stabilized cycle, as seen in the end of Section 2.2. Furthermore, an increase in σ_{L} could be realized through a non-linear backstress having a very high γ_i, such that its settling phase is practically negligible. To minimize these effects (which generate an ill-conditioned inversion), experimental tests should be properly designed, aiming at a single and reproducible identification. It may be a particularly difficult task, as the material parameters are obviously unknown before the tests. However, as only errors in stress-strain space are considered, this fact does not necessarily impair the quality of the identification process.

Since limiting the number of experiments is a concern of practical interest, the identified model will inevitably be more precise at simulating conditions that are similar to the calibration experiments, and this must be considered while designing the procedure. In this specific case, the procedure points towards an accurate modelling of stabilized hysteresis cycles for low-cycle fatigue testing.

For cyclically stable materials, the direct problem may be straightforwardly inverted. In the general case, every experimental test which generates plastic behavior gives rise to both isotropic and kinematic hardening, so that they both concur to the mechanical behavior of the tested specimen. This implies that the experimental stress-strain history is not an output of the direct problem arising from the Chaboche model alone. To separate those

effects and to focus on the kinematic component alone, this identification process only concerns the *stabilized* experimental behavior, where it can be safely assumed that the isotropic hardening has converged to its saturated state. The latter is represented by un unknown value of σ_{L}, which as well is identified from experiments. A suitable isotropic hardening law could be identified separately afterwards, starting from the obtained Chaboche parameters. Thus, the overall complexity of the identification process is significantly reduced. The assumption of saturated isotropic hardening is valid as long as it is quick enough to reach saturation before specimen failure and it does not show memorization effects, which would yield a saturated σ_{L} that depends on strain amplitude and past loading history. On the other hand, if an arbitrarily complex evolution of σ_{L} is already known through other strategies, the developed analytical relations may still be used to identify the kinematic parameters only.

Before the identification, it is necessary to choose a specific form of the Chaboche model, namely the number n of backstress components required to model the tested material. It is actually a *maximum* number of components, since one may always set $C_i = 0$ to remove that component. Since there are no obvious physical hints which point to a specific number of backstress components, this quantity is a source of arbitrariness. A good rule of thumb would be to choose the *simplest* form that can model the experimental behavior with reasonable accuracy. Leaning towards model simplicity, a total number of $n = 3$ backstress components are chosen, divided as follows: a fully non-linear component χ_1, a slightly non-linear component χ_2 and a linear component χ_3 ($\gamma_1 > \gamma_2 > \gamma_3 = 0$). Despite having three backstress components as in the classical Chaboche model (Chaboche, 1986), this model has a subtly different setup. In fact, Chaboche suggested the use of two fully non-linear components and a linear component, as the latter controls the tangent modulus at high strains. On the contrary, in this case only a single backstress component shows a significantly non-linear behavior; the slightly non-linear component is employed to tune the tangent modulus, while the linear component is used to control the value of the stabilized mean stress. Since this may lead to inaccurate material models in some situations, a framework to increase the number of non-linear backstress components is also presented in Section 3.3.

3.1. Procedure description

A total of 7 parameters must be identified: $C_1, C_2, C_3, \gamma_1, \gamma_2, \chi_{3,0}$ and σ_{L}. In fact, recall that $\gamma_3 = 0$ and that $\chi_{1,0}$ and $\chi_{2,0}$ do not affect the stabilized behavior, so only $\chi_{3,0}$ affects stabilized cycles in strain control. Eq. (17) provides an equation containing only C_3 and $\chi_{3,0}$, if a stabilized cycle is available:

$$\chi_{3,0} + C_3 \left(\frac{\varepsilon_{\mathrm{p}}^{\min} + \varepsilon_{\mathrm{p}}^{\max}}{2} \right) = \frac{\sigma_{\mathrm{stab}}^{\min} + \sigma_{\mathrm{stab}}^{\max}}{2} \tag{46}$$

If two stabilized cycles are available, two of Eq. (46) can be joined in a linear system, obtaining C_3 and $\chi_{3,0}$. Note that, in principle, the two stabilized cycles can be obtained from the same specimen, unless failure occurs before completion of the test. The mean plastic strain of the cycle is defined as: $\varepsilon_{\mathrm{p}}^{\mathrm{m}} = (\varepsilon_{\mathrm{p}}^{\min} + \varepsilon_{\mathrm{p}}^{\max})/2$. By using indexes "I" and "II" for the two available experimental cycles, it holds that:

$$\begin{aligned} \chi_{3,0} + C_3\, \varepsilon_{\mathrm{p,I}}^{\mathrm{m}} &= \sigma_{\mathrm{m,I}} \\ \chi_{3,0} + C_3\, \varepsilon_{\mathrm{p,II}}^{\mathrm{m}} &= \sigma_{\mathrm{m,II}} \end{aligned} \tag{47}$$

whose solution is:

$$C_3 = \frac{\sigma_{\mathrm{m,II}} - \sigma_{\mathrm{m,I}}}{\varepsilon^{\mathrm{m}}_{\mathrm{p,II}} - \varepsilon^{\mathrm{m}}_{\mathrm{p,I}}}$$
$$\chi_{3,0} = \frac{\varepsilon^{\mathrm{m}}_{\mathrm{p,II}}\,\sigma_{\mathrm{m,I}} - \varepsilon^{\mathrm{m}}_{\mathrm{p,I}}\,\sigma_{\mathrm{m,II}}}{\varepsilon^{\mathrm{m}}_{\mathrm{p,II}} - \varepsilon^{\mathrm{m}}_{\mathrm{p,I}}} \tag{48}$$

For the system to be well-conditioned, $\varepsilon^{\mathrm{m}}_{\mathrm{p,I}}$ and $\varepsilon^{\mathrm{m}}_{\mathrm{p,II}}$ must be significantly different: in other words, the average strains of the experimental cycles must be sufficiently spaced. As a rule of thumb, setting $\varepsilon^{\mathrm{min}}_{\mathrm{p}} = -\varepsilon^{\mathrm{max}}_{\mathrm{p}}$ for the first cycle and $\varepsilon^{\mathrm{min}}_{\mathrm{p}} = 0$ for the second is usually a good choice. To obtain stabilized cycles, it is advised to carry out cyclic tests in strain control instead of stress control, to avoid ratcheting. The first stabilized cycle shall be large enough to show an approximately linear plastic region, a sign that non-linear backstress components reached saturation.

Eq. (20) provides another condition from the slope at cycle extreme points, involving all C_i and γ_i:

$$\left.\frac{\mathrm{d}\sigma}{\mathrm{d}\varepsilon_{\mathrm{p}}}\right|_{\sigma=\sigma^{\mathrm{max}}_{\mathrm{stab}}} = C_1\left(1 - \tanh\left(\frac{\gamma_1\Delta\varepsilon_{\mathrm{p}}}{2}\right)\right) + C_2\left(1 - \tanh\left(\frac{\gamma_2\Delta\varepsilon_{\mathrm{p}}}{2}\right)\right) + C_3 \tag{49}$$

By assuming that γ_2 is only slightly non-linear, $\gamma_2\Delta\varepsilon_{\mathrm{p}} \ll 1$ will hold in most practical cases, so Eq. (49) becomes:

$$\left.\frac{\mathrm{d}\sigma}{\mathrm{d}\varepsilon_{\mathrm{p}}}\right|_{\sigma=\sigma^{\mathrm{max}}_{\mathrm{stab}}} = C_1\left(1 - \tanh\left(\frac{\gamma_1\Delta\varepsilon_{\mathrm{p}}}{2}\right)\right) + C_2 + C_3 \tag{50}$$

Since at least two cycles are needed for C_3 and $\chi_{3,0}$, two of Eq. (50) will be available. The same stabilized cycles can be used, or, if necessary, any two different cycles.

Note that, if γ_1 was known in advance (as well as C_3, known from Eqs. (48)), the two coefficients C_1 and C_2 could be identified from the resulting linear system:

$$C_1\left(1 - \tanh\left(\frac{\gamma_1\Delta\varepsilon_{\mathrm{p,I}}}{2}\right)\right) + C_2 = -C_3 + \left.\frac{\mathrm{d}\sigma}{\mathrm{d}\varepsilon_{\mathrm{p}}}\right|_{\sigma=\sigma^{\mathrm{max}}_{\mathrm{stab,I}}}$$
$$C_1\left(1 - \tanh\left(\frac{\gamma_1\Delta\varepsilon_{\mathrm{p,II}}}{2}\right)\right) + C_2 = -C_3 + \left.\frac{\mathrm{d}\sigma}{\mathrm{d}\varepsilon_{\mathrm{p}}}\right|_{\sigma=\sigma^{\mathrm{max}}_{\mathrm{stab,II}}} \tag{51}$$

whose solution is:

$$C_1 = \frac{b_{\mathrm{II}} - b_{\mathrm{I}}}{a_{\mathrm{II}} - a_{\mathrm{I}}}$$
$$C_2 = \frac{a_{\mathrm{II}}b_{\mathrm{II}} - a_{\mathrm{I}}b_{\mathrm{I}}}{a_{\mathrm{II}} - a_{\mathrm{I}}} \tag{52}$$

where a_{I} and a_{II} are defined as:

$$a_{\mathrm{I}} = 1 - \tanh\left(\frac{\gamma_1\Delta\varepsilon_{\mathrm{p,I}}}{2}\right)$$
$$a_{\mathrm{II}} = 1 - \tanh\left(\frac{\gamma_1\Delta\varepsilon_{\mathrm{p,II}}}{2}\right) \tag{53}$$

and:

$$b_{\mathrm{I}} = -C_3 + \left.\frac{\mathrm{d}\sigma}{\mathrm{d}\varepsilon_{\mathrm{p}}}\right|_{\sigma=\sigma^{\max}_{\mathrm{stab,I}}}$$
$$b_{\mathrm{II}} = -C_3 + \left.\frac{\mathrm{d}\sigma}{\mathrm{d}\varepsilon_{\mathrm{p}}}\right|_{\sigma=\sigma^{\max}_{\mathrm{stab,II}}} \tag{54}$$

The system of Eqs. (51) is non-singular as long as $a_{\mathrm{I}} \neq a_{\mathrm{II}}$. To be more precise, a well-conditioned system is obtained if the quantities $\tanh\left(\frac{\gamma_1 \Delta\varepsilon_{\mathrm{p,I}}}{2}\right)$ and $\tanh\left(\frac{\gamma_1 \Delta\varepsilon_{\mathrm{p,II}}}{2}\right)$ are significantly different. Since the optimal γ_1 is not known a priori, a physical condition is instead suggested. The first cycle should be just large enough to show an approximately linear plastic flow near its extremities, which would testify that fully non-linear backstress components have saturated. Then, the second cycle should be performed at a significantly lower plastic strain amplitude (something like a half of the previous one). That would yield a not-yet-saturated first component and a significantly different tangent modulus at extremities.

Eq. (18) provides another condition on the stress amplitude of the stabilized cycle, involving all parameters except $\chi_{3,0}$:

$$2\frac{C_1}{\gamma_1}\tanh\left(\frac{\gamma_1 \Delta\varepsilon_{\mathrm{p}}}{2}\right) + 2\frac{C_2}{\gamma_2}\tanh\left(\frac{\gamma_2 \Delta\varepsilon_{\mathrm{p}}}{2}\right) + C_3 \Delta\varepsilon_{\mathrm{p}} + 2\sigma_{\mathrm{L}} = \Delta\sigma \tag{55}$$

From a physical point of view, Eq. (55) relates the plastic strain amplitude with its corresponding stress amplitude, and it can be used to find σ_{L} after having found all the other parameters. The saturated elastic limit can be identified from both stabilized cycles, under the previous assumption that $\gamma_2 \Delta\varepsilon_{\mathrm{p}} \ll 1$:

$$\sigma_{\mathrm{L,I}} = \frac{\Delta\sigma_{\mathrm{I}}}{2} - \frac{C_1}{\gamma_1}\tanh\left(\frac{\gamma_1 \Delta\varepsilon_{\mathrm{p,I}}}{2}\right) - \frac{C_2 + C_3}{2}\Delta\varepsilon_{\mathrm{p,I}}$$
$$\sigma_{\mathrm{L,II}} = \frac{\Delta\sigma_{\mathrm{II}}}{2} - \frac{C_1}{\gamma_1}\tanh\left(\frac{\gamma_1 \Delta\varepsilon_{\mathrm{p,II}}}{2}\right) - \frac{C_2 + C_3}{2}\Delta\varepsilon_{\mathrm{p,II}} \tag{56}$$

These two values are the limit stresses deduced from the full ranges of the two stabilized cycles. If the material actually behaves as supposed by the Chaboche model, the "correct" γ_1 yields $\sigma_{\mathrm{L,I}} = \sigma_{\mathrm{L,II}}$. In practice, that will never occur exactly, so σ_{L} is chosen as the average between the two:

$$\sigma_{\mathrm{L}} = \frac{\sigma_{\mathrm{L,I}} + \sigma_{\mathrm{L,II}}}{2} \tag{57}$$

C_3 and $\chi_{3,0}$ are known, while C_1, C_2 and σ_{L} can be explicitly evaluated if the value of γ_1 is known or assumed. Moreover, γ_2 is assumed small, so it has negligible effects on the stabilized cycles. This means that C_1, C_2 and σ_{L} can be seen as single-variable functions, depending on γ_1. Then, a complete set of parameters (except for γ_2) can be obtained *for each trial value* of γ_1.

An error function Σ can now be introduced, to measure the error in predicting the cycle amplitudes from Eqs. (56) and (57):

$$\Sigma = \left|\frac{\sigma_{\mathrm{L,II}} - \sigma_{\mathrm{L,I}}}{\sigma_{\mathrm{L}}}\right| \tag{58}$$

If $\Sigma = 0$, then $\sigma_{\mathrm{L}} = \sigma_{\mathrm{L,I}} = \sigma_{\mathrm{L,II}}$, so Eqs. (56) are both satisfied at the same time and stress amplitudes are reproduced with no error.

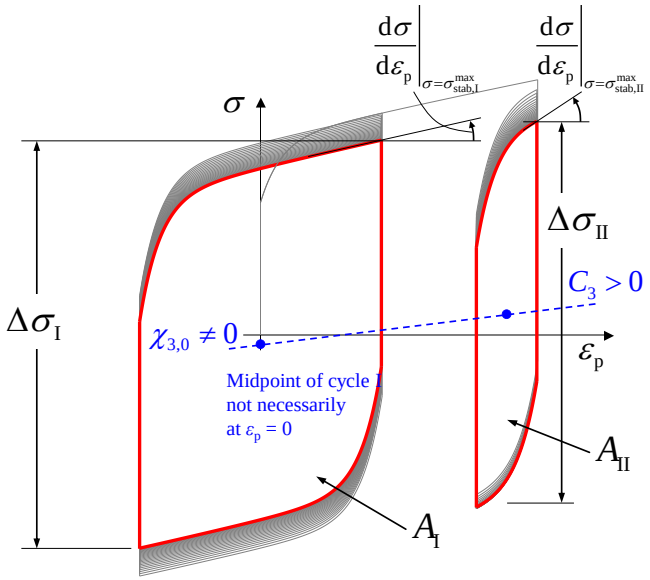

Figure 6: Stabilized cycle properties which are used in the proposed procedure. C_3 and $\chi_{3,0}$ are directly obtained from the linear relation between cycle mean stresses and mean plastic strains. The other overall properties of the cycles are then used for the determination of the other parameters.

Alternatively, one may use a root-mean-square error over the entire cycle, or any other desired quantity. In addition, another term may be added to the error function, to measure the accuracy in reproducing the hysteresis areas. From Eq. (23), and again assuming that $\gamma_2 \Delta\varepsilon_p \ll 1$, the area of the cycle only depends on the first (fully non-linear) backstress component, while the other two provide a contribution in terms of stress amplitude alone, but not in terms of area:

$$A = \oint \sigma \, \mathrm{d}\varepsilon_p = 2\sigma_L \Delta\varepsilon_p + 2\left(\frac{C_1}{\gamma_1}\Delta\varepsilon_p - 2\frac{C_1}{\gamma_1^2}\tanh\left(\frac{\gamma_1 \Delta\varepsilon_p}{2}\right)\right) \tag{59}$$

The relative error on the prediction of the hysteresis area of cycle I can be computed as:

$$\Lambda_I = \frac{2\sigma_L \Delta\varepsilon_{p,I} + 2\left(\frac{C_1}{\gamma_1}\Delta\varepsilon_p - 2\frac{C_1}{\gamma_1^2}\tanh\left(\frac{\gamma_1 \Delta\varepsilon_{p,I}}{2}\right)\right)}{A_I} - 1 \tag{60}$$

where A_I is the experimental value for the hysteresis area of cycle I. The same relative error can be defined for cycle II. A dimensionless error function can now be defined, by incorporating these stress amplitude and hysteresis area relative deviations for both the two cycles in a single expression:

$$\Psi(\gamma_1) = (1-\alpha)\,\Sigma^2 + \alpha(\Lambda_I^2 + \Lambda_{II}^2) \tag{61}$$

where α is a user-defined parameter between 0 and 1, balancing the relative weight of the two error sources. In fact, if $\alpha = 0$, only stress amplitudes are enforced, but that may lead to a significantly different cycle, as will be shown in Section 4. As α is increased towards 1, the accuracy of the cycle extreme points is traded for an improved hysteresis area, which yields a better overall result.

Eventually, γ_1 is chosen as a global minimizer of $\Psi(\gamma_1)$. From a practical point of view, $\Psi(\gamma_1)$ is evaluated at equispaced trial values, belonging to a set of acceptable values. For example, one may test values in the range $100 - 2000$ for most metal alloys. Since all other calculations are analytical, a single value of $\Psi(\gamma_1)$ can be evaluated in negligible time on a common PC and a spreadsheet or numerical software. Fig. 6 summarizes the

minimum set of experimental quantities that are needed to carry out this procedure.

Once that γ_1 is computed, only γ_2 is missing. At a first approximation, it does not affect any stabilized cycle, so it *cannot* be identified from stabilized experimental tests. If only stabilized cycles need to be simulated, γ_2 can be left unknown. For numerical purposes (e.g., FEM analyses), a low value such as $\gamma_2 = 1$ can be assumed. Otherwise, a ratcheting test is required. Specifically, it is necessary to have a test that develops a significant ratcheting behavior, in terms of ratcheting strains but also in terms of cycles before failure. This last requirement is needed to bring $\Delta\varepsilon^{\mathrm{a}}_{\mathrm{p,N}}$ and $\Delta\varepsilon^{\mathrm{s}}_{\mathrm{p,N}}$ to their equilibrium points, past the primary settling phase, where isotropic hardening may be significant too. No explicit prescriptions can be formulated here, since they are material dependent. A load ratio $R = \sigma_{\min}/\sigma_{\max}$ of about -0.7 was found to be a good choice in the present work. In order to take advantage of the linearized version of the equations from Section 2.4, it is desirable that $\gamma_1\Delta\varepsilon^{\mathrm{a}}_{\mathrm{p}} \ll 1$. If this is true, γ_2 can be evaluated from Eq. (38):

$$\gamma_2 = \frac{C_2\Delta\varepsilon^{\mathrm{r}}_{\mathrm{p}}}{2\Delta\varepsilon^{\mathrm{a}}_{\mathrm{p}}\sigma_{\mathrm{m}}} = \frac{C_2\Delta\varepsilon^{\mathrm{s}}_{\mathrm{p}}}{\Delta\varepsilon^{\mathrm{a}}_{\mathrm{p}}\sigma_{\mathrm{m}}} \tag{62}$$

while if it is not, the most appropriate among the first of Eqs. (32), (35) and (36) may be used to obtain γ_2, depending on which approximations are allowed. For example, in a rather common case where $\gamma_1\Delta\varepsilon^{\mathrm{a}}_{\mathrm{p}} \ll 1$ does not hold, but $\gamma_1\Delta\varepsilon^{\mathrm{s}}_{\mathrm{p}} \ll 1$ does, it holds that:

$$\gamma_2 = \frac{\operatorname{asinh}\left(\frac{1}{C_2}\left(\frac{2\sigma_{\mathrm{m}}}{\Delta\varepsilon^{\mathrm{r}}_{\mathrm{p}}} - \frac{C_1}{\sinh(\gamma_1\Delta\varepsilon^{\mathrm{a}}_{\mathrm{p}})}\right)\right)^{-1}}{\Delta\varepsilon^{\mathrm{a}}_{\mathrm{p}}} \tag{63}$$

A *perfectly oblique* linear asymptote will not be available, because of the slight curvature induced by the linear backstress component and because of the last part which leads to specimen failure. Hence, $\Delta\varepsilon^{\mathrm{s}}_{\mathrm{p}}$ shall be determined with sound engineering judgement. As a consistency check on the other parameters, the experimental $\Delta\varepsilon^{\mathrm{a}}_{\mathrm{p}}$ may then be compared with the simulated one. In fact, a mismatch between those quantities would impair the reproduction of $\Delta\varepsilon^{\mathrm{r}}_{\mathrm{p}}$ through Eqs. (62)– (63) and would point towards errors in the reproduction of stabilized cycles. In the event that the experimental $\Delta\varepsilon^{\mathrm{a}}_{\mathrm{p}}$ data is not so accurate, the simulated $\Delta\varepsilon^{\mathrm{a}}_{\mathrm{p}}$ may be alternatively precomputed (as it is practically independent from γ_2) and then introduced into Eqs. (62)–(63).

3.2. Final algorithm

The suggested procedure can be summarized in the following steps:

- Carry out at least two experimental tests in strain control, having different amplitude.
- For each obtained stabilized cycle, record $\Delta\varepsilon_{\mathrm{p}}$, $\varepsilon^{\mathrm{m}}_{\mathrm{p}}$, $\Delta\sigma$, σ_{m}, A and $\mathrm{d}\sigma/\mathrm{d}\varepsilon_{\mathrm{p}}$ at an extreme point.
- Evaluate C_3 and $\chi_{3,0}$ from Eqs. (48).
- Define an array of trial values for γ_1. A good choice might be equispaced samples from 100 to 2000.
- Define an error function $\Psi(C_1, \gamma_1, C_2, \gamma_2, C_3, \chi_{3,0}, \sigma_L)$ which will measure the goodness-of-fit of a parameter set.
- For each trial value of γ_1:
  - Compute a_{I}, a_{II}, b_{I} and b_{II} from Eqs. (53)–(54).
  - Evaluate C_1 and C_2 from Eqs. (52).

  - Compute $\sigma_{\mathrm{L,I}}$ and $\sigma_{\mathrm{L,II}}$ from Eqs. (56).
  - Evaluate σ_{L} from Eq. (57).
  - Compute Ψ for the given trial value.

- Choose γ_1 which globally minimizes Ψ and update other parameters accordingly.
- If γ_2 is not needed, set it to an arbitrary low value; a good choice would be 1.
- If γ_2 is needed, perform an experimental test in stress control, having non-null mean stress σ_{m}.
- Record $\Delta\varepsilon^{\mathrm{a}}_{\mathrm{p},N}$ and $\Delta\varepsilon^{\mathrm{s}}_{\mathrm{p},N}$, then check that these values have practically converged to non-null values $\Delta\varepsilon^{\mathrm{a}}_{\mathrm{p}}$ and $\Delta\varepsilon^{\mathrm{s}}_{\mathrm{p}}$ before failure.
- Evaluate γ_2 from Eq. (62) or Eq. (63), depending on their domain of application. If a plastic shakedown occurred, set γ_2 to an arbitrary low value. A good choice would be in the order of 10^{-2}, to generate a negligible ratcheting.
- If an identification of parameters for a Voce hardening law is needed, fit Q and b in Eq. (45), applied on any of the available tests in strain control.

3.3. Further refinements: additional backstress components

The proposed procedure assumes that the material behavior can be well represented by $n = 3$ backstress components having different dynamics. This number was also suggested by Chaboche himself (Chaboche, 1986), although his arrangement of backstress components is slightly different with respect to the proposed procedure. In fact, a traditional Chaboche kinematic model uses a single linear component, used to model the linear asymptote of the stress-strain curve at high strains. On the other hand, as discussed in Section 2.5, the proposed procedure uses the linear component only for describing the relation between the mean plastic strain and the mean stress, while it uses a slightly non-linear component to tune the asymptotic tangent modulus and the asymptotic ratcheting behavior. In other words, only a single backstress component models the non-linear material behavior after yielding, while at least two of them are usually employed in the "classic" Chaboche model.

Since the extreme points are the only pointwise stress values that are used, the proposed procedure is likely to be less accurate around the elastic limit than it is at extreme points. That is in general a critical zone for the Chaboche model itself, as it cannot reproduce a smooth elastic-plastic transition (Chaboche, 1986). However, a very quick backstress may be used to at least improve the model performance in that zone.

In general, the relations reported in Section 2 can be used as constraints for more complex numerical methods (Nath et al., 2019; Mahmoudi et al., 2011; Badnava et al., 2012; Nath et al., 2021; Chaparro et al., 2008), and the results of the proposed procedure can be employed as a first guess which facilitates the convergence of the solver. Alternatively, a framework for including that additional backstress component is provided in the following.

By running the proposed procedure with $\alpha = 0$ (or approximately so) in Eq. (61), only the peak values are enforced, without constraints on the hysteresis areas. This usually yields a cycle which is more accurate near the extreme points, with bigger deviations at the elastic limit (e.g., see Fig. 11(c) in Section 4). The result may be also controlled by limiting the maximum allowable value of γ_1. Then, the yield zone is refined by trading the introduction of another backstress component (C_4, γ_4) with a *decrease* in σ_L by $\frac{C_4}{\gamma_4}$; by doing so, when the added component saturates to $\frac{C_4}{\gamma_4}$, the simulated curve turns back to the original one. C_4 and γ_4 can be identified

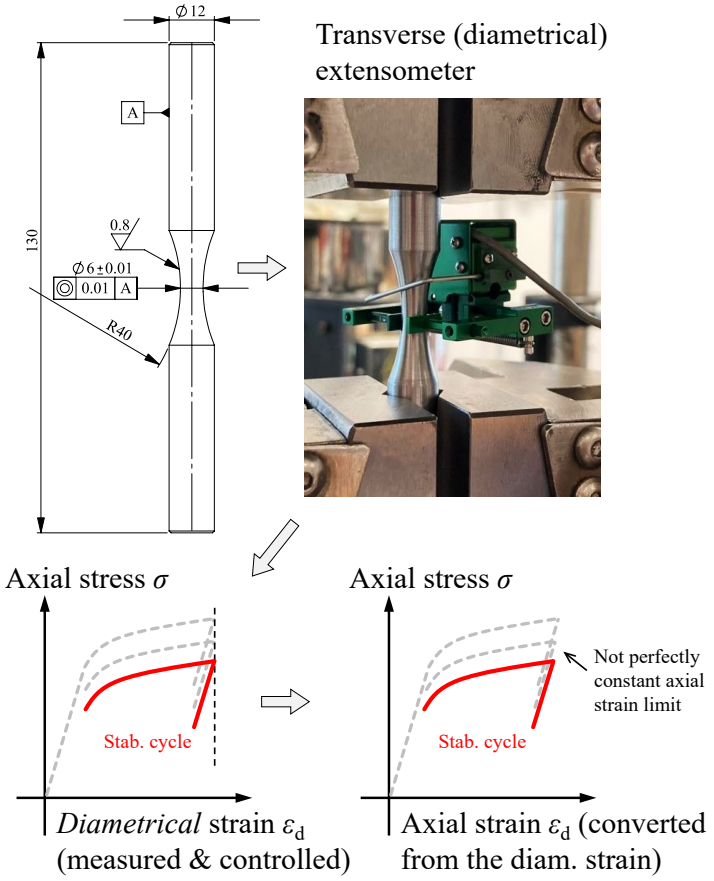

Figure 7: Hourglass specimen and transverse extensometer setup for tests under (diameter) strain control.

by minimizing the hysteresis areas relative error $\Lambda_{\mathrm{I}}^2 + \Lambda_{\mathrm{II}}^2$, though other discrepancy measures can be employed. In mathematical terms:

- Generate a matrix of trial values for C_4 and γ_4.
- For each matrix entry, evaluate the new elastic limit at $\sigma_L - \frac{C_4}{\gamma_4}$.
- Minimize $\Lambda_{\mathrm{I}}^2 + \Lambda_{\mathrm{II}}^2$ (or another functional of choice) over the trial matrix and obtain (C_4, γ_4), together with the updated value of σ_L.

4. Application examples

4.1. Experimental setup

An experimental campaign was conducted on axisymmetric hourglass coupons (illustrated in Fig. 7) with gage diameter of 6 mm, extracted from 60 mm diameter rolled bars. The samples longitudinal axes were aligned with the bars rolling direction.

Cyclic tests were performed on 7075-T6 aluminum, 42CrMo4 steel, and high-silicon ferritic ductile cast iron (Borsato et al., 2021) specimens, according to the standard ASTM E606. A servo-hydraulic universal testing machine INSTRON 8516 was used, equipped with hydraulic grips, a load cell of 100 kN (nonlinearity ±0.1% of R.O.) and a diametrical (transversal) extensometer (nonlinearity ±0.15% of R.O.). When strain-controlled, each sample was subjected to strain cycles with constant amplitude, through triangular waveforms having a constant

strain rate of $10^{-2}\mathrm{s}^{-1}$. The axial strain ε was deduced from the diametrical one ε_d according to the following equation prescribed by ASTM E606, assuming plastic incompressibility:

$$\varepsilon = \frac{\sigma}{E}(1-2\nu) - 2\varepsilon_\mathrm{d} \tag{64}$$

where for 7075-T6 aluminum $E = 70.5$ GPa and $\nu = 0.33$, for 42CrMo4+QT steel $E = 206$ GPa and $\nu = 0.3$, while for high-silicon ductile cast iron $E = 170$ GPa and $\nu = 0.27$. Stress-controlled tests where carried out through feedback on load cell measurements.

4.2. Aluminum alloy 7075-T6

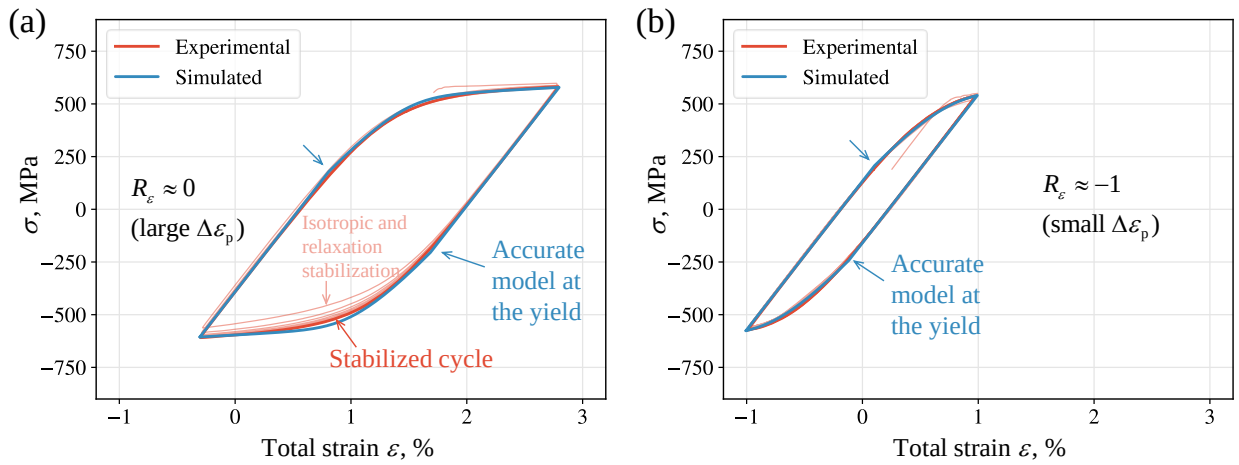

Figure 8: Determination of the Chaboche kinematic hardening model parameters for the aluminum alloy 7075-T6. Stabilized cycles are shown in (a) and (b), having different strain ratios and strain amplitudes.

First, the use of the proposed procedure is presented for the aluminum 7075-T6 results. This material showed an almost negligible isotropic hardening, therefore the determination of the Voce's equation parameters was not performed, i.e. a purely kinematic model ($\sigma_0 = \sigma_\mathrm{L}$) was assumed. Moreover, for this alloy, no ratcheting test was available. Then, the parameter γ_2 was not determined, and $\gamma_2 = 1$ was assumed, according to Section 3.2. Fig. 8 shows the two stabilized cycles that were required for the other parameters to be determined. As evident in the figure and discussed above, in order to have a well conditioned identification problem, these two cycles significantly differ in terms of strain ratio R_ε, thus allowing a well-conditioned determination of the linear backstress constant C_3. The two cycles also differ in terms of plastic strain amplitude, therefore the derivatives at the extremities are quite dissimilar. This, in turn, allows an efficient extraction of the other two coefficients C_1 and C_2 as functions of γ_1. Eventually, the latter was obtained by equially weighting errors on the peak stress values and on the hysteresis areas ($\alpha = 0.5$). It is quite evident that the yield region is accurately represented, as well as the post-yield segment of both ramps. Recall that this result was obtained just imposing the *global* parameters of the cycles. The identified parameters are reported in Table 1. Recall that γ_2^* is not the result of an identification, but rather a conventional value, since ratcheting tests were not carried out. Due to this, it has been denoted with an asterisk.

Table 1: Results of the proposed procedure for 7075-T6 specimens, in terms of identified parameters.

C_1	γ_1	C_2	γ_2^*	C_3	$\chi_{3,0}$	σ_L
126 GPa	707	2.83 GPa	1	349 MPa	−18.1 MPa	392 MPa

4.3. Steel 42CrMo4+QT

Two samples of steel 42CrMo4+QT were tested at two different strain ratios R_ε, namely -1 and 0, to produce axial strain amplitudes of, respectively, about 2.8% and 1.7%, until a stabilized cycle was achieved. Stress-strain histories for the two strain-controlled tests are plotted in Fig. 9.

The first specimen (having $R_\varepsilon \approx -1$) was subjected to 100 load cycles; then, a stabilized cycle was practically evident, so the specimen was saved for the subsequent ratcheting test. The second specimen (having $R_\varepsilon \approx 0$) was tested until failure. Its stabilized cycle was then identified as a minimum in the change rate of cycle extreme points.

In addition, a ratcheting test was performed on the first specimen, after the strain-controlled test. For this purpose, the maximum axial load $P_{\max}$ of the stabilized cycle was recorded, then the sample was cycled in load control between the maximum value $P_{\max}$ and the minimum value $-0.75P_{\max}$ ($R = -0.75$). These load values correspond to axial stresses ranging between -538 MPa and 718 MPa. The stress-strain history of the ratcheting test is reported in Fig. 10(a), from which the ratcheting curve (maximum strain vs. cycle) was extracted. The latter is reported in Fig. 10(b).

The ratcheting curve shows the typical three phases found by other authors (Kang, 2008; Paul, 2012): a first settling phase, an approximately linear phase, and a last phase where the ratcheting rate increases until failure. The appropriate ratcheting rate to be fed to Eq. (63) is identified at the beginning of the second phase (around the 20th cycle), where it is assumed that $\Delta\varepsilon^{\mathrm{s}}_{\mathrm{p},N}$ has practically converged and that the linear backstress component has still a negligible effect. Its value is $\Delta\varepsilon^{\mathrm{r}}_{\mathrm{p}} = 2\Delta\varepsilon^{\mathrm{s}}_{\mathrm{p}} = 822$ με/cycle. The quantities needed for the application of the procedure are reported in Table 2.

The procedure is carried out according to Section 3.2. The obtained Chaboche parameters are reported in Table 3. For the sake of clarity, in Fig. 11 the effects of some procedure parameters are reported.

The error function defined in Eq. (61) has been used, setting $\alpha = 0.5$. Experimental tests were simulated with the obtained model and compared with measurements. Strain-controlled tests are depicted in Fig. 9, while the experimental ratcheting and predicted curve (with tuned γ_2) are reported in Fig. 10(b). Moreover, in Fig. 12 some experimental and simulated ratcheting cycles are compared in the $\sigma - \varepsilon$ plane.

Voce parameters are identified by fitting Q and b in Eq. (45), applied to the lower amplitude cycle. The experimental history of σ_Y vs. p is reported in Fig. 13. Values of $Q = -120.5$ and $b = 0.733$ are obtained. Novak et al. (2020) reported similar values of Q and b for this material.

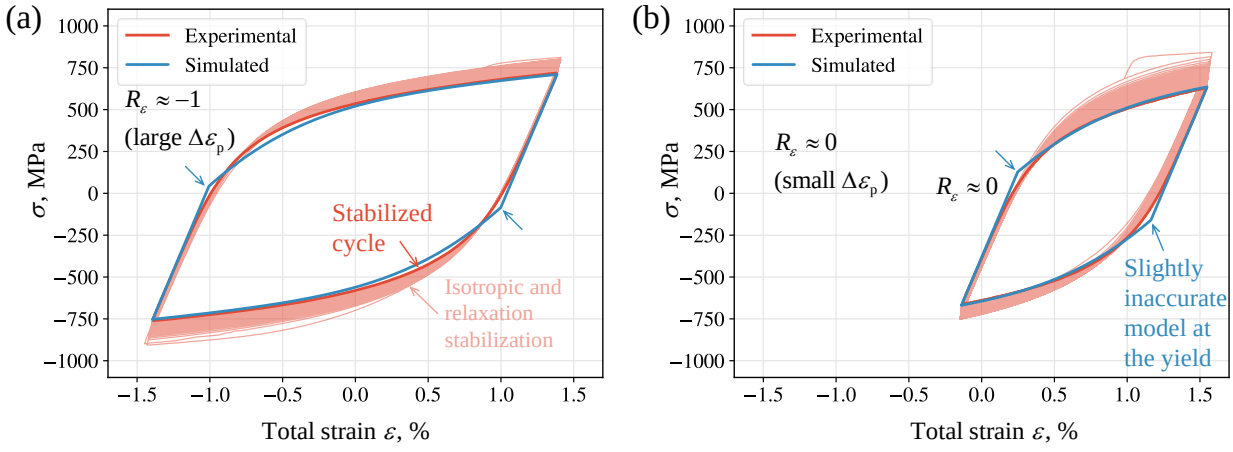

Figure 9: Experimental tests under strain control. Stabilized cycles are highlighted in red. (a) Test at $R_\varepsilon \approx -1$. (b) Test at $R_\varepsilon \approx 0$.

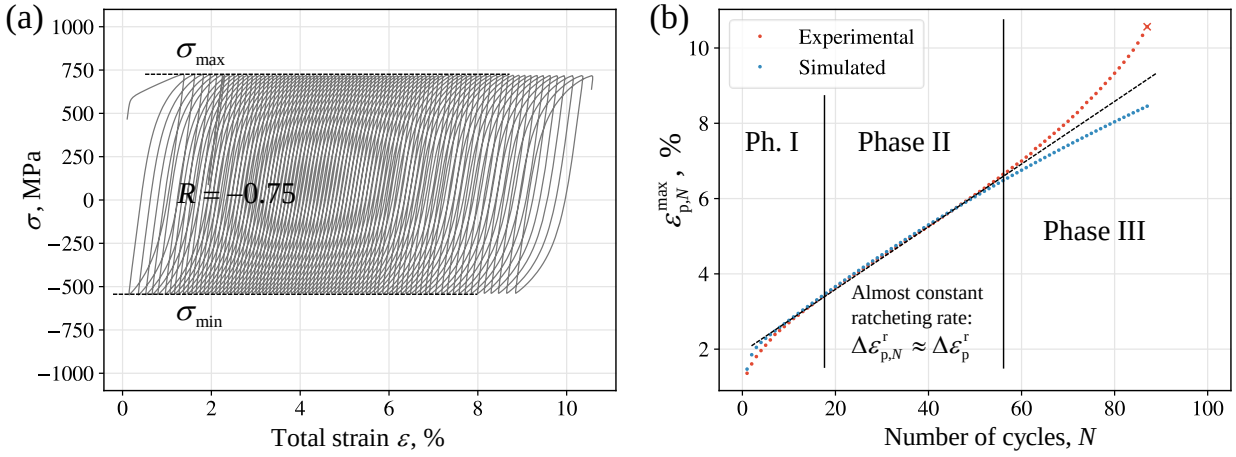

Figure 10: Ratcheting test in stress control. (a) Experimental stress-strain curve. (b) Evolution of maximum strain $\varepsilon^{\max}_{p,N}$ with respect to cycle number N. Three separate ratcheting phases can be identified. In phase I the ratcheting rate is decreasing, in phase II the ratcheting rate converges to an approximately constant value $\Delta\varepsilon^{r}_{p,N} \approx \Delta\varepsilon^{r}_{p}$ (linear phase), while in phase III the ratcheting rate increases until specimen failure.

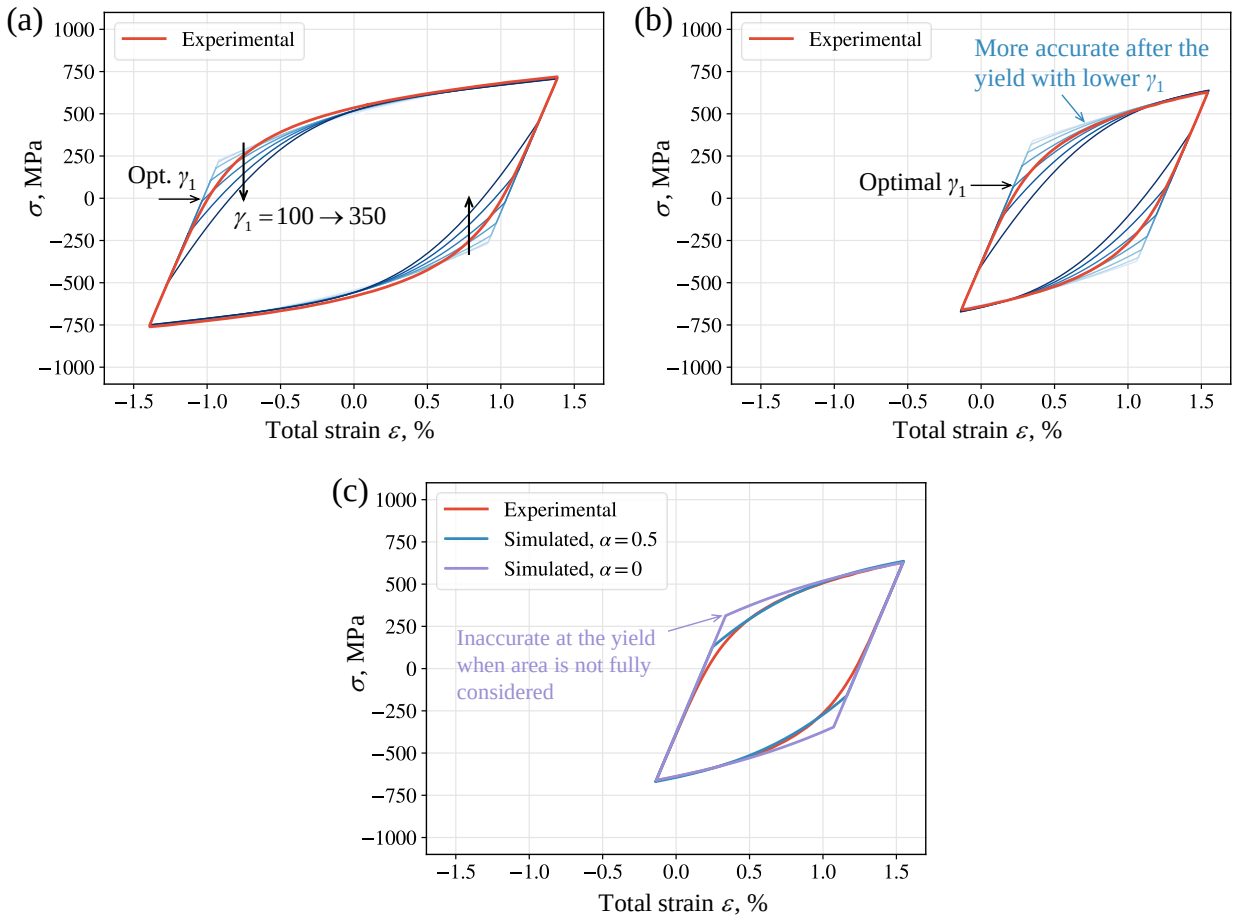

Figure 11: (a)–(b) Sweep of stabilized cycles obtained by varying γ_1 with respect to the actual minimizer of $\Psi(\gamma_1)$, respectively for the higher and lower strain amplitude. (c) If the hysteresis area of the cycle is not considered in $\Psi(\gamma_1)$ (by setting $\alpha = 0$), the obtained stabilized cycle becomes inaccurate at the yielding zone.

As suggested in Section 3.3, an identification with $n = 4$ backstress components was also obtained, for reference. The procedure was carried out with $n = 3$ and $\alpha = 0$, as in Fig. 11(c), then a fourth component was added by minimizing the relative errors $\Lambda_I^2 + \Lambda_{II}^2$ in describing the hysteresis areas. The complete set of

Table 2: Global properties extracted from experimental tests, used as inputs for the proposed procedure.

Stabilized cycle I	$\Delta\varepsilon_{p,I}$	2.07%
	$\varepsilon^{m}_{p,I}$	0.01%
	$\Delta\sigma_{I}$	1479 MPa
	$\sigma_{m,I}$	−21.06 MPa
	A_{I}	23.08 mJ/mm^3
	$d\sigma/d\varepsilon_p$ at $\sigma = \sigma^{max}_{stab,I}$	10.09 GPa
Stabilized cycle II	$\Delta\varepsilon_{p,II}$	1.0%
	$\varepsilon^{m}_{p,II}$	0.71%
	$\Delta\sigma_{II}$	1288 MPa
	$\sigma_{m,II}$	−16.51 MPa
	A_{II}	9.81 mJ/mm^3
	$d\sigma/d\varepsilon_p$ at $\sigma = \sigma^{max}_{stab,II}$	17.89 GPa
Ratcheting test	σ_m	92.79 MPa
	$\Delta\varepsilon^{a}_{p}$	7977 με
	$\Delta\varepsilon^{s}_{p}$	411 με

Table 3: Results of the proposed procedure for 42CrMo4+QT specimens, in terms of identified parameters.

C_1	γ_1	C_2	γ_2	C_3	$\chi_{3,0}$	σ_L
57.5 GPa	238	8.62 GPa	5.18	643 MPa	−21.1 MPa	398 MPa

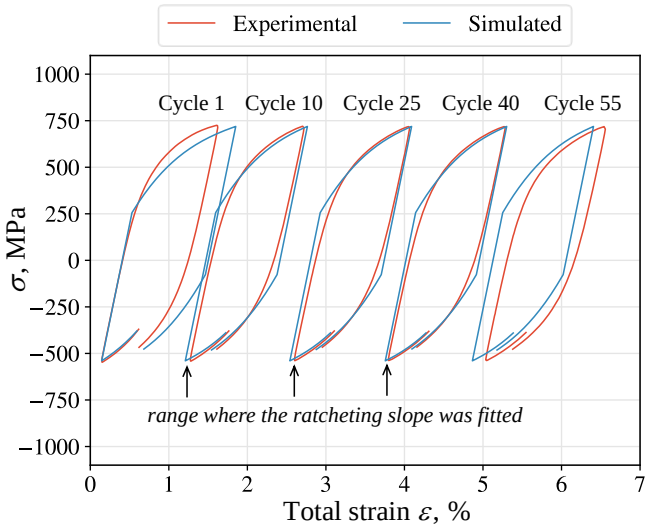

Figure 12: Comparison of experimental and simulated cycles drawn from the ratcheting test. For clarity, only some cycles are reported.

parameters (kinematic and isotropic) for the identification with 4 backstress components is reported in Table 4, and the corresponding stabilized cycles are reported in Fig. 14.

Table 4: Complete set of parameters for the CIKH model after introducing the isotropic and 4-th backstress component.

C_1	γ_1	C_2	γ_2	C_3	$\chi_{3,0}$	C_4	γ_4	σ_L	Q	b
27.1 GPa	117	5.01 GPa	3.13	643 MPa	−21.1 MPa	109 GPa	714	334 MPa	−122 MPa	0.686

4.4. High-silicon ferritic ductile cast iron

Two samples of high-silicon ferritic ductile cast iron were tested in strain control, with amplitudes of about 1.2% and 0.75%. Both the strain ratios R_ε were set at approximately −1. In principle, this is in contrast with

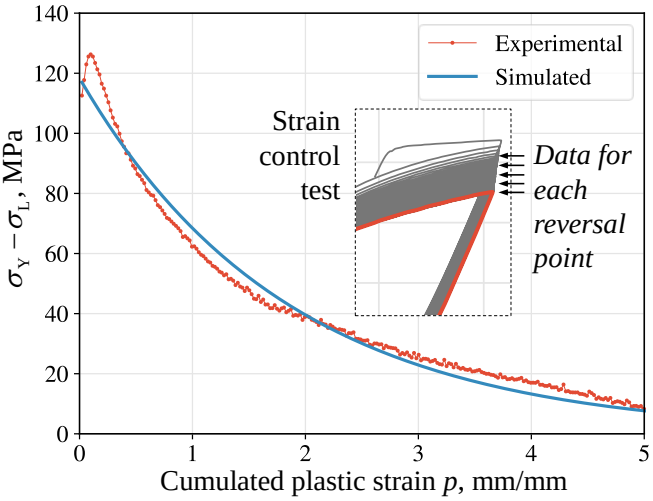

Figure 13: Experimental history of σ_Y vs. p, used to fit the Q and b parameters of Voce hardening law.

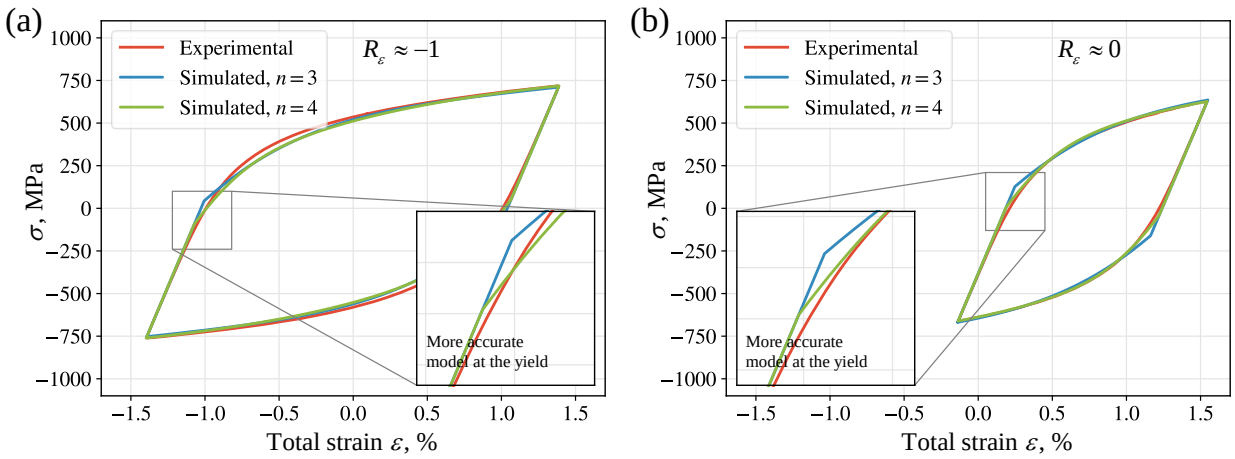

Figure 14: Further refinement of the obtained results, achieved by adding a fourth highly-dynamic backstress component.

the recommendations of Section 3; however, in this specific case the system (47) was still reasonably well-conditioned, and that allowed the identification of the linear backstress component. These tests are reported in Fig. 15(a). To identify the slightly non-linear backstress component, a ratcheting test was also performed on the first specimen, after the strain-controlled test. Axial stresses ranged between −298 MPa and 523 MPa, and the corresponding ratcheting curve is reported in Fig.16.

The full procedure with 4 backstress components was carried out, according to Sections 3.2 and 3.3. The corresponding simulated tests are shown in Fig. 15(a) and Fig. 16. The parameters for a Voce isotropic hardening were identified by fitting Q and b in Eq. (45), analyzing the load history of the test with higher strain amplitude. The final set of parameters is reported in Table 5.

After the identification of a complete CIKH model, additional tests were performed to validate the obtained parameters. Another specimen was tested in strain-control, with an amplitude of about 1%. Its experimental stress-strain history is reported in Fig. 15(b), together with its simulated stabilized cycle. Its entire stress-strain history is also simulated with the obtained CIKH model, and the simulated trend of the maximum peak stress values is compared with the experimental values in Fig. 17. Two more specimens were tested in stress-control, with stress ranges of −284 to 504 MPa and −291 to 484 MPa. Their corresponding ratcheting curves are reported in Fig. 16, with their simulated counterparts.

Table 5: Complete set of parameters for the CIKH model for the high-silicon ferritic ductile cast iron. A 4-backstress identification was performed.

C_1	γ_1	C_2	γ_2	C_3	$\chi_{3,0}$	C_4	γ_4	σ_L	Q	b
82.1 GPa	841	12.1 GPa	13.5	1124 MPa	42.1 MPa	798 GPa	4538	172 MPa	39.3 MPa	5.02

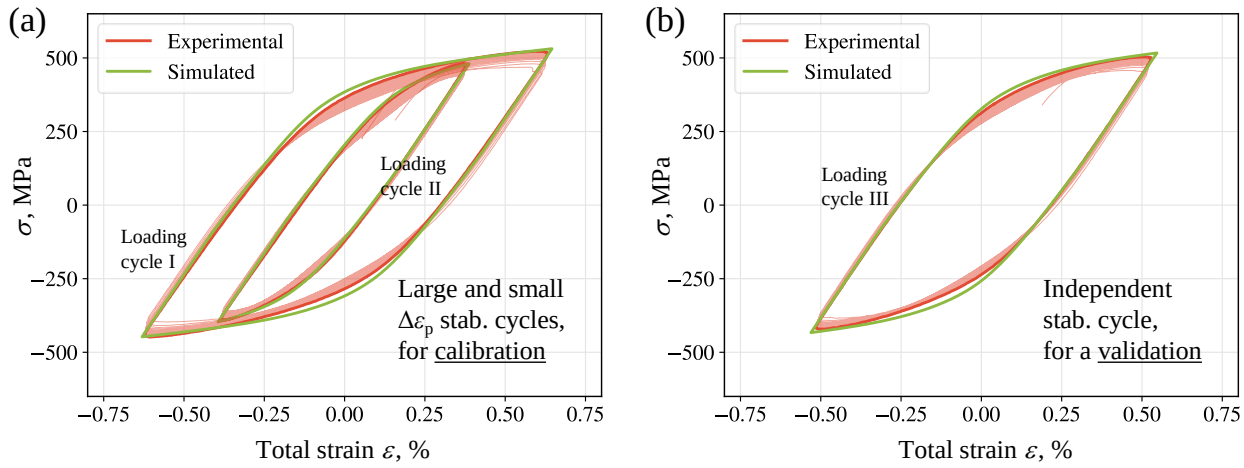

Figure 15: (a) Experimental strain-controlled cyclic tests used to calibrate the Chaboche parameters. The simulated stabilized cycles are reported in green. (b) Additional strain-controlled test used to validate the obtained model.

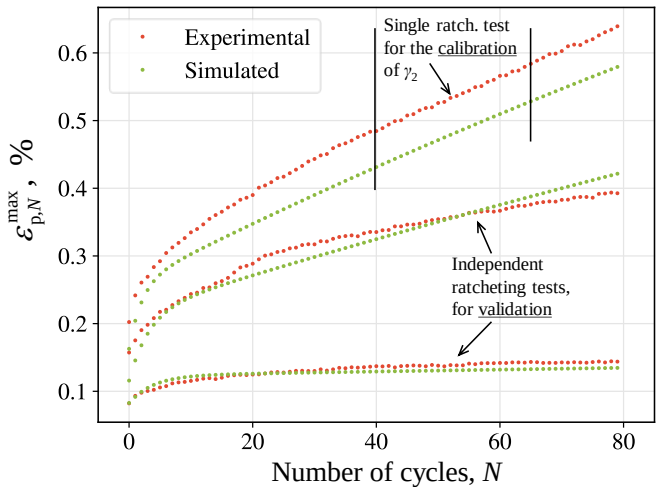

Figure 16: Ratcheting curves corresponding to the three stress-controlled tests. The test with higher stress amplitude was used to calibrate the model, while the other two tests serve as a validation of the obtained parameters.

5. Discussion

5.1. General considerations

Since the system composed by Eqs. (51) was solved exactly, the tangent moduli at the extreme points were reproduced perfectly by the identified set of parameters, at least for the strain amplitudes of the experimental tests. The same can be said for average stresses and average strains, because of Eqs. (48). On the other hand, the error function involving hysteresis areas and stress amplitudes is minimized to a value that is non-null in general, therefore those two quantities are reproduced with some errors. As evident in Figs. 8, 9 and 15, these errors are barely appreciable and negligible in engineering practice. As anticipated in the Introduction, the parameters were identified with a *deterministic* process from the experimental tests.

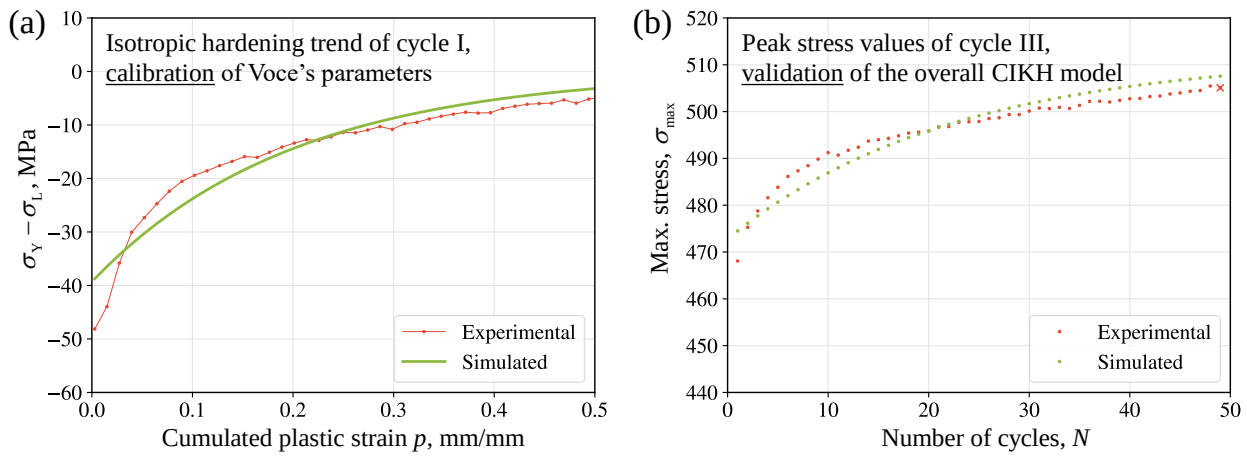

Figure 17: (a) Calibration of a Voce isotropic hardening law on the stress history of the first strain-controlled test. (b) Correlation between experimental and simulated peak stress history on the third strain-controlled test, used for validation.

Table 6: Accuracy in the reproduction of stress amplitudes and hysteresis areas for the two 42CrMo4+QT experimental stabilized cycles.

Stabilized cycle I	Experimental	Simulated	Variation
$\Delta\sigma_{\mathrm{I}}$	1479 MPa	1463 MPa	−1.08%
A_{I}	23.1 mJ/mm^3	22.5 mJ/mm^3	−2.60%
Stabilized cycle II	**Experimental**	**Simulated**	**Variation**
$\Delta\sigma_{\mathrm{II}}$	1288 MPa	1304 MPa	1.23%
A_{II}	9.81 mJ/mm^3	10.06 mJ/mm^3	2.55%

5.2. Aluminum alloy 7075-T6

As ratcheting tests were not available, the procedure assumed a low γ_2, in this case equal to 1. Its effect on the tangent slope at extremities is thus that of a linear backstress, although it avoids the corresponding effect on the shift of cycle mean stress values. Note in Fig. 8 that the simulation of stabilized cycles for aluminum 7075-T6 is particularly accurate. This fact *does not imply* that a ratcheting test would be accurately predicted by the obtained parameters. As shown in Section 2.4 and in Fig. 18(b), the ratcheting behavior is mainly governed by the rate value of the smallest non-linear backstress component (namely, γ_2), whereas it has almost no influence on the stabilized cycles, as long as $\gamma_2 \Delta\varepsilon_{\mathrm{p}} \ll 1$. Therefore, the obtained model can be expected to work well in predicting other stabilized cycles, but should not be used for stress-controlled tests.

5.3. Steel 42CrMo4+QT

The steel 42CrMo4+QT was characterized by both strain- and stress-controlled cycles. Two strain-controlled cycles and a single ratcheting test were available, which is the minimum set of tests required to carry out the entire procedure proposed. Starting with the input data in Table 2, the stabilized cycles in Fig. 9 were obtained, and a detailed analysis of the identification errors is reported in Table 6. Despite some slight inaccuracies near the elastic limit, all relative errors were below 3%. The cycles were reproduced very accurately especially near the peak stress values. In our opinion, this level of accuracy is more than enough to use the constitutive model obtained as an input for other applications such as fatigue life models. As shown in Fig. 13, the model obtained can then be easily paired with a Voce isotropic hardening law. Except for the first few cycles, where the evolution of the elastic limit does not seem to follow an exponential law, the Voce law describes the material behavior well. A complete CIKH model was thus obtained deterministically and in almost negligible computational time.

The accuracy in reproducing the ratcheting test is notable, especially because the only imposed condition is the slope of its approximately linear phase, which is used to tune γ_2. In fact, the simulated test is very close to the

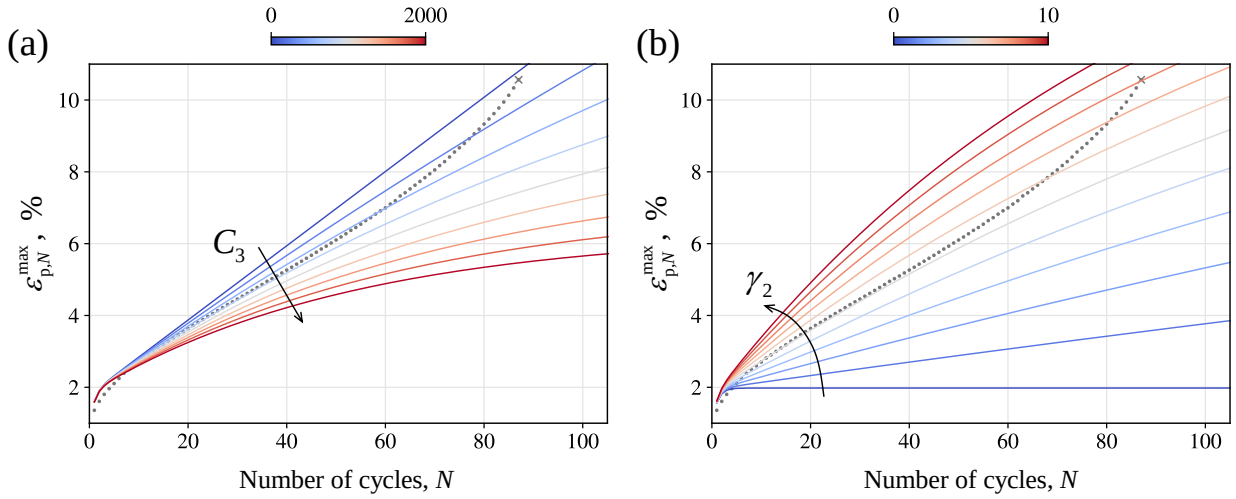

Figure 18: Effect of C_3 and of γ_2 on the simulated ratcheting curve. (a) C_3 is varied between 0 and 2000 MPa while C_2 is updated accordingly to maintain the same tangent modulus at high strains. All other parameters in Table 3 are kept constant. At C_3 = 2000 MPa the concavity of the ratcheting curve is significantly higher than the experimental one. (b) γ_2 is varied between 0 and 10. All other parameters in Table 3 are kept constant.

experimental one, not only in terms of maximum cycle strain (see Fig. 10) but also in the shape and amplitude of the translating hysteresis cycle (see Fig. 12) which has a lower amplitude than the calibration cycles. This supports the hypothesis that the model is consistent with the material behavior. In fact, no information on the shape of the ratcheting cycle was given as input to the procedure. Only the asymptotic ratcheting rate was used, while the cycle shape followed from the parameters obtained through the stabilized cycles. As discussed in Section 2.5, the last part of the ratcheting curve with an increasing ratcheting rate cannot be reproduced with the Chaboche model in this uniaxial framework, at least not without taking potential geometry changes in the specimen into account, as observed in (Paul, 2012).

The effects of variations of C_3 on the ratcheting simulations are reported in Fig. 18(a). If the reproduction of the tangent modulus at high strains had been performed using C_3 only, a value near 9345 MPa (current value of $C_2 + C_3$) would have been obtained, which would have produced unmanageable concavity of the ratcheting curve (see Fig. 18 (a)) and the reproduction of the experimental test would not have been possible. This effect has already been observed, for example in (Ramezansefat and Shahbeyk, 2015). In contrast, the proposed procedure yielded a much smaller C_3, which is still compatible with the experimental data. Fig. 18(b) shows an example of how γ_2 affects ratcheting curves. Note that values of γ_2 in the considered range have negligible effects on stabilized cycles.

By setting $\alpha = 0.5$ in the error function of Eq. (61), the hysteresis areas of stabilized cycles were enforced. A practical explanation can be found in Fig. 11(c), where the smaller simulated cycle is compared with the results obtained with $\alpha = 0$. Although the extreme points are always well reproduced, by also minimizing errors on hysteresis areas, the simulated cycle is forced to be extremely close to the experimental cycle also at intermediate strain values.

The addition of another backstress component (starting with the parameters obtained with $\alpha = 0$) yields a more accurate prediction of the mechanical behavior in the yield zone, as shown in Fig. 14. Since the prediction with three backstresses is already fairly accurate, the increased complexity of the procedure should be evaluated on a case-by-case basis.

5.4. High-silicon ferritic ductile cast iron

Since the tangent moduli are always reproduced exactly, the obtained Chaboche parameters should be able to model moderate amplitude variations accurately, at least with a first approximation. In addition, as two experimental cycles are provided, it is also reasonable to expect that intermediate amplitudes are modeled reliably.

This hypothesis was tested with the experimental campaign on a high-silicon ferritic ductile cast iron. After the complete procedure was carried out (including the additional fourth backstress component), the obtained model was validated with additional experimental tests. An additional strain-controlled cycle was performed at an intermediate (but significantly different) amplitude between the two calibration cycles. As shown in Fig. 15(b), the stabilized cycle is well predicted, with an accuracy that is comparable with that of the calibration cycles.

Three ratcheting tests were also performed, although only the asymptotic ratcheting rate of the one with the highest amplitude was used to calibrate the parameter γ_2. Some interesting conclusions can be drawn from Fig. 16. In fact, the procedure yields a set of parameters that satisfies a constraint on the *asymptotic ratcheting rate*, however the point-wise absolute value of the ratcheting strain is not guaranteed to match the experimental data. In fact, the CIKH model obtained for the high-silicon ferritic ductile cast iron yields a ratcheting curve that is slightly shifted with respect to the calibrating test (see Fig. 16). Compared with the highly accurate ratcheting prediction of Fig. 10 for the steel 42CrMo4+QT, its relative error is higher, but in absolute terms it represents a moderate discrepancy (see the different Y-scale in Fig. 16). By correctly predicting the asymptotic slope, this error also remains approximately constant across multiple stress cycles.

On the other hand, the prediction accuracy for the two additional validation cycles is notable. The one with the intermediate amplitude is well reproduced, except for a slight discrepancy in the asymptotic ratcheting rate. The one with the lowest amplitude is reproduced with almost no error at all, both in terms of absolute ratcheting strain and ratcheting rate.

The isotropic hardening is well reproduced by a Voce law (see Fig. 17), although in this case a pure exponential form is probably not the best function to fit the experimental data. However, errors are limited to a maximum of approximately 10 MPa. When the overall CIKH model is used to predict the peak stress values of the independent strain-controlled cycle, as in Fig. 17(b), a similar accuracy is achieved, and the trend is well predicted.

6. Conclusions

This work explores a possible analytical procedure for the identification of Chaboche parameters. Analytical expressions for asymptotic ratcheting rates in uniaxial tests are provided. By attempting to identify a Chaboche model with three backstress components, one of which is assumed to be linear, while another is assumed to be only *slightly* non-linear, an almost fully analytical procedure is proposed. The aim is to reproduce some *global* quantities of stabilized cycles which are often important for the prediction of other phenomena such as fatigue. The only numerical part involves the minimization of a single-variable function, depending on γ_1. As the latter can be reasonably assumed to lie in a given interval, this process is particularly easy and can also be done with a common spreadsheet file. The proposed procedure uses the hysteresis area, cycle peak stress values and slope at extreme points as inputs. However, the framework can be adapted to minimize the error evaluated on any other desired property, by defining an appropriate error function.

Although only global conditions are imposed, the model identified actually achieves a great correlation over the entire range of the ramps of the stabilized cycles. Even though the results are validated in a uniaxial

setting, the stabilized behavior is believed to still be satisfactory in multiaxial conditions with a dominant stress component or at least under proportional loadings. In addition, the uniaxial ratcheting is accurately reproduced with various input conditions, though only its asymptotic slope is imposed. This highlights the self-consistency of the identified model, and relating the ratcheting slope to the model parameters is an innovative contribution of this work.

The Chaboche model parameters were obtained with a *deterministic* process and without any manual tuning, which is a strong point of the procedure. As shown, the obtained model could still be improved by adding more (highly dynamic) backstress components, if necessary. It should be underlined that the proposed procedure runs in negligible computational time on a typical personal computer.

Although more refined models may be more accurate at predicting the material behavior in a variety of different conditions, they often need an extensive experimental campaign to be calibrated. In contrast, this procedure only requires three tests (possibly on the same specimen) to identify the full parameter set of a CIKH model. This is a particularly advantageous feature for example when the main target of a study is to characterize the fatigue behavior of new materials (e.g., regarding their notch sensitivity). In fact, most of the fatigue life under proportional loading is usually spent under stabilized conditions, which are the main focus of this procedure.

The analytical relations obtained may also be used as constraints for any of the other identification algorithms available in the literature, and the obtained parameters could even be introduced as reliable initial values to attain numerical convergence. In addition, the approach of imposing a correct prevision on independent loading conditions is recommended to optimize the determination of the parameters of any other material model or constitutive equation.

References

Abdel-Karim, M., 2010. An evaluation for several kinematic hardening rules on prediction of multiaxial stress-controlled ratchetting. International Journal of Plasticity 26, 711–730. doi:10.1016/j.ijplas.2009.10.002.

Abueidda, D.W., Koric, S., Sobh, N.A., Sehitoglu, H., 2021. Deep learning for plasticity and thermo-viscoplasticity. International Journal of Plasticity 136, 102852. doi:10.1016/j.ijplas.2020.102852.

Agius, D., Kajtaz, M., Kourousis, K.I., Wallbrink, C., Wang, C.H., Hu, W., Silva, J., 2017. Sensitivity and optimisation of the Chaboche plasticity model parameters in strain-life fatigue predictions. Materials and Design 118, 107–121. doi:10.1016/j.matdes.2017.01.027.

Ansys, I., 2013. ANSYS Mechanical APDL Theory Reference. Ansys, Inc. Release 15.0.

Armstrong, P.J., Frederick, C.O., 1966. A mathematical representation of the multiaxial Bauschinger effect. Technical Report C.E.G.B. Report RD/B/N731. Berkeley Nuclear Laboratories, Berkeley, UK.

Arora, P., Samal, M.K., Gupta, S.K., Chattopadhyay, J., 2021. Proposing an improved cyclic plasticity material model for assessment of multiaxial response of low C-Mn steel. International Journal of Fatigue 142, 105888. doi:10.1016/j.ijfatigue.2020.105888.

Badnava, H., Pezeshki, S.M., Nejad, K.F., Farhoudi, H.R., 2012. Determination of combined hardening material parameters under strain controlled cyclic loading by using the genetic algorithm method. Journal of Mechanical Science and Technology 26, 3067–3072. doi:10.1007/s12206-012-0837-1.

Bandyopadhyay, R., Gustafson, S.E., Kapoor, K., Naragani, D., Pagan, D.C., Sangid, M.D., 2021. Comparative assessment of backstress models using high-energy X-ray diffraction microscopy experiments and crystal plasticity finite element simulations. International Journal of Plasticity 136, 102887. doi:10.1016/j.ijplas.2020.102887.

Bari, S., Hassan, T., 2000. Anatomy of coupled constitutive models for ratcheting simulation. International Journal of Plasticity 16, 381–409. doi:10.1016/s0749-6419(99)00059-5.

Bemfica, C., Castro, F., 2021. A cyclic plasticity model for secondary hardening due to strain-induced martensitic transformation. International Journal of Plasticity 140, 102969. doi:10.1016/j.ijplas.2021.102969.

Benedetti, M., Berto, F., Le Bone, L., Santus, C., 2020. A novel Strain-Energy-Density based fatigue criterion accounting for mean stress and plasticity effects on the medium-to-high-cycle uniaxial fatigue strength of plain and notched components. International Journal of Fatigue 133, 105397. doi:10.1016/j.ijfatigue.2019.105397.

Bertini, L., Le Bone, L., Santus, C., Chiesi, F., Tognarelli, L., 2017. High Load Ratio Fatigue Strength and Mean Stress Evolution of Quenched and Tempered 42CrMo4 Steel. Journal of Materials Engineering and Performance 26, 3784–3793. doi:10.1007/s11665-017-2845-x.

Borsato, T., Ferro, P., Fabrizi, A., Berto, F., Carollo, C., 2021. Long solidification time effect on solution strengthened ferritic ductile iron fatigue properties. International Journal of Fatigue 145, 106137.

Branco, R., Prates, P.A., Costa, J.D., Berto, F., Kotousov, A., 2018. New methodology of fatigue life evaluation for multiaxially loaded notched components based on two uniaxial strain-controlled tests. International Journal of Fatigue 111, 308–320. doi:10.1016/j.ijfatigue.2018.02.027.

Broggiato, G.B., Campana, F., Cortese, L., 2008. The Chaboche nonlinear kinematic hardening model: calibration methodology and validation. Meccanica 43, 115–124. doi:10.1007/s11012-008-9115-9.

Burgold, A., Droste, M., Seupel, A., Budnitzki, M., Biermann, H., Kuna, M., 2020. Modeling of the cyclic deformation behavior of austenitic TRIP-steels. International Journal of Plasticity 133, 102792. doi:10.1016/j.ijplas.2020.102792.

Cao, W., Yang, J., Zhang, H., 2021. Unified constitutive modeling of Haynes 230 including cyclic hardening/softening and dynamic strain aging under isothermal low-cycle fatigue and fatigue-creep loads. International Journal of Plasticity 138, 102922. doi:10.1016/j.ijplas.2020.102922.

Chaboche, J.L., 1986. Time-independent constitutive theories for cyclic plasticity. International Journal of Plasticity 2, 149–188.

Chaboche, J.L., 2008. A review of some plasticity and viscoplasticity constitutive theories. International Journal of Plasticity 24, 1642–1693. doi:10.1016/j.ijplas.2008.03.009.

Chaboche, J.L., Jung, O., 1997. Application of a kinematic hardening viscoplasticity model with thresholds to the residual stress relaxation. International Journal of Plasticity 13, 785–807. doi:10.1016/s0749-6419(97)00066-1.

Chaboche, J.L., Kanouté, P., Azzouz, F., 2012. Cyclic inelastic constitutive equations and their impact on the fatigue life predictions. International Journal of Plasticity 35, 44–66. doi:10.1016/j.ijplas.2012.01.010.

Chaparro, B.M., Thuillier, S., Menezes, L.F., Manach, P.Y., Fernandes, J.V., 2008. Material parameters identification: Gradient-based, genetic and hybrid optimization algorithms. Computational Materials Science 44, 339–346. doi:10.1016/j.commatsci.2008.03.028.

Cheong, M.F.L.W., Rouse, J.P., Hyde, C.J., Kennedy, A.R., 2018. The Prediction of isothermal cyclic plasticity in 7175-T7351 aluminium alloy with particular emphasis on thermal ageing effects. International Journal of Fatigue 114, 92–108. doi:10.1016/j.ijfatigue.2018.05.010.

Das, B., Paul, S.K., Singh, A., Arora, K.S., Shome, M., 2020. The effect of thickness variation and pre-strain on the cornering fatigue life prediction of a DP600 steel wheel disc. International Journal of Fatigue 139, 105799. doi:10.1016/j.ijfatigue.2020.105799.

Ding, J., Kang, G., Kan, Q., Liu, Y., 2012. Constitutive model for uniaxial time-dependent ratcheting of 6061-T6 aluminum alloy. Constitutive model for uniaxial time-dependent ratcheting of 6061-T6 57, 67–72. doi:10.1016/j.commatsci.2011.06.015.

Djimli, L., Taleb, L., Meziani, S., 2010. The role of the experimental data base used to identify material parameters in predicting the cyclic plastic response of an austenitic steel. International Journal of Pressure Vessels and Piping 87, 177–186. doi:10.1016/j.ijpvp.2010.02.002.

Egner, W., Sulich, P., Mroziński, S., Egner, H., 2020. Modelling thermo-mechanical cyclic behavior of P91 steel. International Journal of Plasticity 135, 102820. doi:10.1016/j.ijplas.2020.102820.

Esmaeili, A., Walia, M.S., Handa, K., Ikeuchi, K., Ekh, M., Vernersson, T., Ahlström, J., 2017. A methodology to predict thermomechanical cracking of railway wheel treads: From experiments to numerical predictions. International Journal of Fatigue 105, 71–85. doi:10.1016/j.ijfatigue.2017.08.003.

Fu, J., Barlat, F., Kim, J.H., Pierron, F., 2016. Identification of nonlinear kinematic hardening constitutive model parameters using the virtual fields method for advanced high strength steels. International Journal of Solids and Structures 102-103, 30–43. doi:10.1016/j.ijsolstr.2016.10.020.

Hai, L.T., Li, G.Q., Wang, Y.B., Wang, Y.Z., 2021. A fast calibration approach of modified Chaboche hardening rule for low yield point steel, mild steel and high strength steels. Journal of Building Engineering 38, 102168. doi:10.1016/j.jobe.2021.102168.

Hamidinejad, S.M., Varvani-Farahani, A., 2015. Ratcheting assessment of steel samples under various non-proportional loading paths by means of kinematic hardening rules. Materials and Design 85, 367–376. doi:10.1016/j.matdes.2015.06.153.

Han, J., Marimuthu, K.P., Koo, S., Lee, H., 2020. Numerical implementation of modified Chaboche kinematic hardening model for multiaxial ratcheting. Computers and Structures 231, 106222. doi:10.1016/j.compstruc.2020.106222.

Hansen, P.C., 2010. Discrete Inverse Problems. Society for Industrial and Applied Mathematics. doi:10.1137/1.9780898718836.

Hassan, T., Kyriakides, S., 1992. Ratcheting in cyclic plasticity, part I: Uniaxial behaviour. International Journal of Plasticity 8, 91–116.

Hassan, T., Taleb, L., Krishna, S., 2008. Influence of non-proportional loading on ratcheting responses and simulations by two recent cyclic plasticity models. International Journal of Plasticity 24, 1863–1889. doi:10.1016/j.ijplas.2008.04.008.

Hwang, J.H., Kim, H.T., Kim, Y.J., Nam, H.S., Kim, J.W., 2020. Crack tip fields at crack initiation and growth under monotonic and large amplitude cyclic loading: Experimental and FE analyses. International Journal of Fatigue 141, 105889. doi:10.1016/j.ijfatigue.2020.105889.

Jiang, Y., Zhang, J., 2008. Benchmark experiments and characteristic cyclic plasticity deformation. International Journal of Plasticity 24, 1481–1515.

Kang, G., 2008. Ratchetting: Recent progresses in phenomenon observation, constitutive modeling and application. International Journal of Fatigue 30, 1448–1472. doi:10.1016/j.ijfatigue.2007.10.002.

Kang, G., Liu, Y., Ding, J., 2008. Multiaxial ratchetting–fatigue interactions of annealed and tempered 42CrMo steels: Experimental observations. International Journal of Fatigue 30, 2104–2118. doi:10.1016/j.ijfatigue.2008.06.002.

Kang, G., Liu, Y., Ding, J., Gao, Q., 2009. Uniaxial ratcheting and fatigue failure of tempered 42CrMo steel: Damage evolution and damage-coupled visco-plastic constitutive model. International Journal of Plasticity 25, 838–860. doi:10.1016/j.ijplas.2008.06.004.

Koo, S., Han, J., Marimuthu, K.P., Lee, H., 2019. Determination of Chaboche combined hardening parameters with dual backstress for ratcheting evaluation of AISI 52100 bearing steel. International Journal of Fatigue 122, 152–163. doi:10.1016/j.ijfatigue.2019.01.009.

Kreethi, R., Mondal, A.K., Dutta, K., 2017. Ratcheting fatigue behaviour of 42CrMo4 steel under different heat treatment conditions. Materials Science & Engineering A 679, 66–74. doi:10.1016/j.msea.2016.10.019.

Lee, C.H., Van Do, V.N., Chang, K.H., 2014. Analysis of uniaxial ratcheting behavior and cyclic mean stress relaxation of a duplex stainless steel. International Journal of Plasticity 62, 17–33. doi:10.1016/j.ijplas.2014.06.008.

Li, H., Yu, C., Kang, G., 2022a. Crystal plasticity modeling of the multiaxial ratchetting of extruded AZ31 Mg alloy. International Journal of Plasticity 152, 103242. doi:10.1016/j.ijplas.2022.103242.

Li, X., Roth, C.C., Bonatti, C., Mohr, D., 2022b. Counterexample-trained neural network model of rate and temperature dependent hardening with dynamic strain aging. International Journal of Plasticity 151, 103218. doi:10.1016/j.ijplas.2022.103218.

Liu, S., Liang, G., Yang, Y., 2019. A strategy to fast determine Chaboche elasto-plastic model parameters by considering ratcheting. International Journal of Pressure Vessels and Piping 172, 251–260. doi:10.1016/j.ijpvp.2019.01.017.

Mahmoudi, A.H., Pezeshki-Najafabadi, S.M., Badnava, H., 2011. Parameter determination of Chaboche kinematic hardening model using a multi objective Genetic Algorithm. Computational Materials Science 50, 1114–1122. doi:10.1016/j.commatsci.2010.11.010.

Mohammadpour, A., Chakherlou, T.N., 2016. Numerical and experimental study of an interference fitted joint using a large deformation Chaboche type combined isotropic–kinematic hardening law and mortar contact method. International Journal of Mechanical Sciences 106, 297–318. doi:10.1016/j.ijmecsci.2015.10.012.

Moslemi, N., Mozafari, F., Abdi, B., Gohari, S., Redzuan, N., Burvill, C., Ayob, A., 2020. Uniaxial and biaxial ratcheting behavior of pressurized AISI 316L pipe under cyclic loading: Experiment and simulation. International Journal of Mechanical Sciences 179, 105693. doi:10.1016/j.ijmecsci.2020.105693.

Nath, A., Barai, S.V., Ray, K.K., 2021. Studies on the experimental and simulated cyclic-plastic response of structural mild steels. Journal of Constructional Steel Research 182, 106652. doi:10.1016/j.jcsr.2021.106652.

Nath, A., Ray, K.K., Barai, S.V., 2019. Evaluation of ratcheting behaviour in cyclically stable steels through use of a combined kinematic-isotropic hardening rule and a genetic algorithm optimization technique. International Journal of Mechanical Sciences 152, 138–150. doi:10.1016/j.ijmecsci.2018.12.047.

Novak, J.S., Franulović, M., Benasciutti, D., De Bona, F., 2020. Modeling the cyclic plasticity behavior of 42CrMo4 steel with an isotropic model calibrated on the whole shape of the evolution curve. Procedia Structural Integrity 28, 53–60. doi:10.1016/j.prostr.2020.10.007.

Okorokov, V., Gorash, Y., Mackenzie, D., van Rijswick, R., 2019. New formulation of nonlinear kinematic hardening model, Part II: Cyclic hardening/softening and ratcheting. International Journal of Plasticity 122, 244–267. doi:10.1016/j.ijplas.2019.07.005.

Paul, S.K., 2012. Effect of anisotropy on ratcheting: An experimental investigation on IFHS steel sheet. Materials Science and Engineering: A 538, 349–355. doi:10.1016/j.msea.2012.01.058.

Paul, S.K., 2016. Numerical models of plastic zones and associated deformations for a stationary crack in a C(T) specimen loaded at different R-ratios. Theoretical and Applied Fracture Mechanics 84, 183–191. doi:10.1016/j.tafmec.2015.10.008.

Paul, S.K., 2019. A critical review of experimental aspects in ratcheting fatigue: microstructure to specimen to component. Journal of Materials Research and Technology 8, 4894–4914. doi:10.1016/j.jmrt.2019.06.014.

Paul, S.K., 2020. Correlation between endurance limit and cyclic yield stress determined from low cycle fatigue test. Materialia 11, 100695. doi:10.1016/j.mtla.2020.100695.

Paul, S.K., Majumdar, S., Kundu, S., 2014. Low cycle fatigue behavior of thermo-mechanically treated rebar. Materials & Design 58, 402–411. doi:10.1016/j.matdes.2014.01.079.

Paul, S.K., Sivaprasad, S., Dhar, S., Tarafder, S., 2010. Ratcheting and low cycle fatigue behavior of SA333 steel and their life prediction. Journal of Nuclear Materials 401, 17–24. doi:10.1016/j.jnucmat.2010.03.014.

Paul, S.K., Tarafder, S., 2013. Cyclic plastic deformation response at fatigue crack tips. International Journal of Pressure Vessels and Piping 101, 81–90. doi:10.1016/j.ijpvp.2012.10.007.

Ramezansefat, H., Shahbeyk, S., 2015. The Chaboche hardening rule: A re-evaluation of calibration procedures and a modified rule with an evolving material parameter. Mechanics Research Communications 69, 150–158. doi:10.1016/j.mechrescom.2015.08.003.

Rokhgireh, H., Nayebi, A., Chaboche, J.L., 2017. Application of a new distortional yield surface model in cyclic uniaxial and multiaxial loading. International Journal of Solids and Structures 110-111, 219–238. doi:10.1016/j.ijsolstr.2017.01.026.

Shekarian, A., Varvani-Farahani, A., 2019. Ratcheting Prediction at the Notch Root of Steel Samples Over Asymmetric Loading Cycles. Journal of Engineering Materials and Technology 142. doi:10.1115/1.4045363.

Shekarian, A., Varvani-Farahani, A., 2021. Ratcheting behavior of notched stainless steel samples subjected to asymmetric loading cycles. Journal of Iron and Steel Research International 28, 86–97. doi:10.1007/s42243-020-00465-2.

Sinaie, S., Heidarpour, A., Zhao, X.L., 2014. A multi-objective optimization approach to the parameter determination of constitutive plasticity models for the simulation of multi-phase load histories. Computers and Structures 138, 112–132. doi:10.1016/j.compstruc.2014.03.005.

Song, Z., Komvopoulos, K., 2014. An elastic–plastic analysis of spherical indentation: Constitutive equations for single-indentation unloading and development of plasticity due to repeated indentation. Mechanics of Materials 76, 93–101. doi:10.1016/j.mechmat.2014.05.005.

Voce, E., 1948. The relationship between stress and strain for homogeneous deformations. Journal of the Institute of Metals 74, 537–562.

Wagoner, R.H., Lim, H., Lee, M.G., 2013. Advanced Issues in springback. International Journal of Plasticity 45, 3–20. doi:10.1016/j.ijplas.2012.08.006.

Wójcik, M., Skrzat, A., 2020. Fuzzy logic enhancement of material hardening parameters obtained from tension–compression test. Continuum Mechanics and Thermodynamics 32, 959–969. doi:10.1007/s00161-019-00805-y.

Wójcik, M., Skrzat, A., 2021. Identification of Chaboche–Lemaitre combined isotropic–kinematic hardening model parameters assisted by the fuzzy logic analysis. Acta Mechanica 232, 685–708. doi:10.1007/s00707-020-02851-z.

Xie, X.F., Jiang, W., Chen, J., Zhang, X., Tu, S.T., 2019. Cyclic hardening/softening behavior of 316L stainless steel at elevated temperature including strain-rate and strain-range dependence: Experimental and damage-coupled constitutive modeling. International Journal of Plasticity 114, 196–214. doi:10.1016/j.ijplas.2018.11.001.

Xu, L., Nie, X., Fan, J., Tao, M., Ding, R., 2016. Cyclic hardening and softening behavior of the low yield point steel BLY160: Experimental response and constitutive modeling. International Journal of Plasticity 78, 44–63. doi:10.1016/j.ijplas.2015.10.009.

Xu, X., Wang, Z., Zhang, X., Gao, G., Wang, P., Kan, Q., 2022. Strain amplitude-dependent cyclic softening behavior of carbide-free bainitic rail steel: Experiments and modeling. International Journal of Fatigue 161, 106922. doi:10.1016/j.ijfatigue.2022.106922.

Xue, L., Shang, D.G., Li, D.H., Xia, Y., 2021. Unified Elastic–Plastic Analytical Method for Estimating Notch Local Strains in Real Time under Multiaxial Irregular Loading. Journal of Materials Engineering and Performance doi:10.1007/s11665-021-06085-5.

Yang, H., Zhang, W., Zhuang, X., Zhao, Z., 2020. Calibration of Chaboche Combined Hardening Model for Large Strain Range. Procedia Manufacturing 47, 867–872. doi:10.1016/j.promfg.2020.04.272.

Yuenyong, J., Uthaisangsuk, V., 2020. Micromechanics based modelling of fatigue crack initiation of high strength steel. International Journal of Fatigue 139, 105762. doi:10.1016/j.ijfatigue.2020.105762.

Zakavi, S.J., Zehsaz, M., Eslami, M.R., 2010. The ratchetting behavior of pressurized plain pipework subjected to cyclic bending moment with the combined hardening model. Nuclear Engineering and Design 240, 726–737. doi:10.1016/j.nucengdes.2009.12.012.

Zhang, B., Wang, R., Hu, D., Jiang, K., Hao, X., Mao, J., Jing, F., 2020. Constitutive modelling of ratcheting behaviour for nickel-based single crystal superalloy under thermomechanical fatigue loading considering microstructure evolution. International Journal of Fatigue 139, 105786. doi:10.1016/j.ijfatigue.2020.105786.

Zhang, J., Jiang, Y., 2008. Constitutive modeling of cyclic plasticity deformation of a pure polycrystalline copper. International Journal of Plasticity 24, 1890–1915.

Zhang, S.L., Xuan, F.Z., 2017. Interaction of cyclic softening and stress relaxation of 9–12% Cr steel under strain-controlled fatigue-creep condition: Experimental and modeling. International Journal of Plasticity 98, 45–64. doi:10.1016/j.ijplas.2017.06.007.

Zhao, P., Lu, T.Y., Gong, J.G., Xuan, F.Z., Berto, F., 2021. A strain energy density based life prediction model for notched components in low cycle fatigue regime. International Journal of Pressure Vessels and Piping 193, 104458. doi:10.1016/j.ijpvp.2021.104458.

Zhou, J., Sun, Z., Kanouté, P., Retraint, D., 2018. Experimental analysis and constitutive modelling of cyclic behaviour of 316L steels including hardening/softening and strain range memory effect in LCF regime. International Journal of Plasticity 107, 54–78. doi:10.1016/j.ijplas.2018.03.013.

Zhu, Y., Kang, G., Kan, Q., Bruhns, O.T., Liu, Y., 2016. Thermo-mechanically coupled cyclic elasto-viscoplastic constitutive model of metals: Theory and application. International Journal of Plasticity 79, 111–152. doi:10.1016/j.ijplas.2015.12.005.

Zobec, P., Klemenc, J., 2021. Application of a nonlinear kinematic-isotropic material model for the prediction of residual stress relaxation under a cyclic load. International Journal of Fatigue 150, 106290. doi:10.1016/j.ijfatigue.2021.106290.

Appendix A. Derivation of analytical expressions for hysteresis area, ramp slope and ratcheting rate

Appendix A.1. Hysteresis Area

By denoting the linear backstress component with the usual special index k, from Eqs. (3) and (4) the hysteresis area of a stabilized cycle can be expressed as:

$$A = \oint \sigma \, \mathrm{d}\varepsilon_\mathrm{p} = \int_{\varepsilon_\mathrm{p}^\mathrm{min}}^{\varepsilon_\mathrm{p}^\mathrm{max}} \left(\sum_{i=1 \; i\neq k}^{n} \chi_i + \chi_k + \sigma_\mathrm{L} \right) \mathrm{d}\varepsilon_\mathrm{p} + \int_{\varepsilon_\mathrm{p}^\mathrm{max}}^{\varepsilon_\mathrm{p}^\mathrm{min}} \left(\sum_{i=1 \; i\neq k}^{n} \chi_i + \chi_k - \sigma_\mathrm{L} \right) \mathrm{d}\varepsilon_\mathrm{p} = \tag{A.1}$$

$$= 2\sigma_\mathrm{L} \Delta\varepsilon_\mathrm{p} + \sum_{i=1 \; i\neq k}^{n} \int_{\varepsilon_\mathrm{p}^\mathrm{min}}^{\varepsilon_\mathrm{p}^\mathrm{max}} \chi_i \, \mathrm{d}\varepsilon_\mathrm{p} + \sum_{i=1 \; i\neq k}^{n} \int_{\varepsilon_\mathrm{p}^\mathrm{max}}^{\varepsilon_\mathrm{p}^\mathrm{min}} \chi_i \, \mathrm{d}\varepsilon_\mathrm{p} + \int_{\varepsilon_\mathrm{p}^\mathrm{min}}^{\varepsilon_\mathrm{p}^\mathrm{max}} \chi_k \, \mathrm{d}\varepsilon_\mathrm{p} + \int_{\varepsilon_\mathrm{p}^\mathrm{max}}^{\varepsilon_\mathrm{p}^\mathrm{min}} \chi_k \, \mathrm{d}\varepsilon_\mathrm{p}$$

The terms in Eq. (A.1) can be individually evaluated. Since χ_k is on a biunivocal relationship with ε_p (see Eq. (9)), it follows that:

$$\int_{\varepsilon_\mathrm{p}^\mathrm{max}}^{\varepsilon_\mathrm{p}^\mathrm{min}} \chi_k \, \mathrm{d}\varepsilon_\mathrm{p} = - \int_{\varepsilon_\mathrm{p}^\mathrm{min}}^{\varepsilon_\mathrm{p}^\mathrm{max}} \chi_k \, \mathrm{d}\varepsilon_\mathrm{p} \tag{A.2}$$

In fact, a linear backstress component does not contribute to the area of the hysteresis cycle.

In the ascending ramp $\mathrm{d}\varepsilon_\mathrm{p} > 0$, so the first of Eqs. (6) holds, which can be rewritten as:

$$\chi_i \mathrm{d}\varepsilon_\mathrm{p} = \frac{C_i}{\gamma_i} \mathrm{d}\varepsilon_\mathrm{p} - \frac{1}{\gamma_i} \mathrm{d}\chi_i \tag{A.3}$$

which, integrated, becomes:

$$\int_{\varepsilon_\mathrm{p}^\mathrm{min}}^{\varepsilon_\mathrm{p}^\mathrm{max}} \chi_i \mathrm{d}\varepsilon_\mathrm{p} = \frac{C_i}{\gamma_i}\Delta\varepsilon_\mathrm{p} - \frac{\chi_{j,\mathrm{stab}}^\mathrm{max} - \chi_{j,\mathrm{stab}}^\mathrm{min}}{\gamma_i} = \frac{C_i}{\gamma_i}\Delta\varepsilon_\mathrm{p} - 2\frac{C_i}{\gamma_i^2}\tanh\left(\frac{\gamma_i\Delta\varepsilon_\mathrm{p}}{2}\right) \tag{A.4}$$

With similar considerations, it can be shown that:

$$\int_{\varepsilon_\mathrm{p}^\mathrm{min}}^{\varepsilon_\mathrm{p}^\mathrm{max}} \chi_i \mathrm{d}\varepsilon_\mathrm{p} = \int_{\varepsilon_\mathrm{p}^\mathrm{max}}^{\varepsilon_\mathrm{p}^\mathrm{min}} \chi_i \mathrm{d}\varepsilon_\mathrm{p} \tag{A.5}$$

In other words, the ascending and descending ramps equally contribute to the hysteresis area.

By substituting in Eq. (A.1), the total hysteresis area is found:

$$\oint \sigma \, \mathrm{d}\varepsilon_\mathrm{p} = 2\sigma_\mathrm{L}\Delta\varepsilon_\mathrm{p} + 2\sum_{i=1\ i\neq k}^{n}\left(\frac{C_i}{\gamma_i}\Delta\varepsilon_\mathrm{p} - 2\frac{C_i}{\gamma_i^2}\tanh\left(\frac{\gamma_i\Delta\varepsilon_\mathrm{p}}{2}\right)\right) \tag{A.6}$$

Appendix A.2. Tangent modulus at cycle extreme points

From the first of Eqs. (6), for $\mathrm{d}\varepsilon_\mathrm{p} > 0$ it holds:

$$\left.\frac{\mathrm{d}\chi_i}{\mathrm{d}\varepsilon_\mathrm{p}}\right|_{\chi_i=\chi_{i,\mathrm{stab}}^\mathrm{max}} = C_i - \gamma_i\chi_{i,\mathrm{stab}}^\mathrm{max} = C_i\left(1 - \tanh\left(\frac{\gamma_i\Delta\varepsilon_\mathrm{p}}{2}\right)\right) \tag{A.7}$$

Deriving Eq. (3) and substituting Eq. (A.7):

$$\left.\frac{\mathrm{d}\sigma}{\mathrm{d}\varepsilon_\mathrm{p}}\right|_{\sigma=\sigma^\mathrm{max}} = \sum_{i=1}^{n}\left.\frac{\mathrm{d}\chi_i}{\mathrm{d}\varepsilon_\mathrm{p}}\right|_{\chi_i=\chi_{i,\mathrm{stab}}^\mathrm{max}} = \sum_{i=1\ i\neq k}^{n} C_i\left(1 - \tanh\left(\frac{\gamma_i\Delta\varepsilon_\mathrm{p}}{2}\right)\right) + C_k \tag{A.8}$$

The index k could be left in the sum (having $\gamma_k = 0$ in the hyperbolic tangent terms), but it was left alone for the sake of clarity. The same value can be obtained for the end point of the descending ramp.

Note that differentiability at yield of the stress-strain curve cannot be obtained. In fact, that would require Eq. (A.8) to tend to infinity as $\Delta\varepsilon_\mathrm{p} \to 0$, which cannot be satisfied.

Appendix A.3. Rate of convergence to plastic shakedown

When a linear backstress component is present, a plastic shakedown is the only equilibrium state and the first of Eqs. (32) cannot be used to estimate the smallest non-linear backstress component. In fact, there will be ratcheting only until a point where the linear backstress component reaches an average value that is equal to the mean cyclic stress. There will be a primary phase where non-linear backstress components are settling and potentially an isotropic hardening occurs. Then, the cycle will stabilize its overall shape as non-linear backstress components reach their equilibrium extreme points: in this phase ratcheting may be reasonably approximated as a translation of the equilibrium cycle (though, strictly speaking, the latter is still open). Some considerations can be made on the convergence rate of $\Delta\varepsilon_{\mathrm{p},N}^\mathrm{s}$ to 0, which allows an identification of the smallest non-linear backstress component.

As experimental evidence, confirmed by numerical simulations, it is supposed that $\Delta\varepsilon_{\mathrm{p},N}^\mathrm{a}$ has reached an approximately constant value $\Delta\varepsilon_\mathrm{p}^\mathrm{a}$ and that $\Delta\varepsilon_\mathrm{p}^\mathrm{s}$ tends to 0 with a geometric convergence rate, that is:

$$\Delta\varepsilon_{\mathrm{p},N}^\mathrm{s} = B\omega^N \tag{A.9}$$

where $B \neq 0$ and $0 < \omega < 1$. Just for convenience, express ω as $\exp(-G\Delta\varepsilon_{\mathrm{p}}^{\mathrm{a}})$ with $G > 0$, so that Eq. (A.9) becomes:

$$\Delta\varepsilon_{\mathrm{p},N}^{\mathrm{s}} = B\exp(-G\Delta\varepsilon_{\mathrm{p}}^{\mathrm{a}}N) \tag{A.10}$$

Since $\Delta\varepsilon_{\mathrm{p},N}^{\mathrm{s}} \to 0$, at some point the approximation $1-\exp(-\gamma_i\Delta\varepsilon_{\mathrm{p},N}^{\mathrm{s}}) \approx \gamma_i\Delta\varepsilon_{\mathrm{p},N}^{\mathrm{s}}$ will be sufficiently precise, independently from the magnitude of γ_i. Therefore, Eqs. (29) and (39) can be rewritten as:

$$\begin{aligned}
\chi_{i,N+1}^{\max} &= \exp(-2\gamma_i\Delta\varepsilon_{\mathrm{p}}^{\mathrm{a}})\chi_{i,N}^{\max} + 2C_i\exp(-\gamma_i\Delta\varepsilon_{\mathrm{p}}^{\mathrm{a}})\Delta\varepsilon_{\mathrm{p},N}^{\mathrm{s}} + \frac{C_i}{\gamma_i}(1-\exp(-\gamma_i\Delta\varepsilon_{\mathrm{p}}^{\mathrm{a}}))^2 \\
\chi_{i,N+1}^{\min} &= \exp(-2\gamma_i\Delta\varepsilon_{\mathrm{p}}^{\mathrm{a}})\chi_{i,N}^{\min} + 2C_i\exp(-\gamma_i\Delta\varepsilon_{\mathrm{p}}^{\mathrm{a}})\Delta\varepsilon_{\mathrm{p},N}^{\mathrm{s}} + \frac{C_i}{\gamma_i}(1-\exp(-\gamma_i\Delta\varepsilon_{\mathrm{p}}^{\mathrm{a}}))^2 \\
\chi_{k,N+1}^{\max} &= \chi_{k,N}^{\max} + 2C_k\Delta\varepsilon_{\mathrm{p},N}^{\mathrm{s}} \\
\chi_{k,N+1}^{\min} &= \chi_{k,N}^{\min} + 2C_k\Delta\varepsilon_{\mathrm{p},N}^{\mathrm{s}}
\end{aligned} \tag{A.11}$$

The quantity $\chi_{i,N}^{\mathrm{m}} = (\chi_{i,N}^{\min} + \chi_{i,N}^{\max})/2$ is defined. Eqs. (A.11) can be combined as follows:

$$\chi_{i,N+1}^{\mathrm{m}} = 2C_i\exp(-\gamma_i\Delta\varepsilon_{\mathrm{p}}^{\mathrm{a}})\Delta\varepsilon_{\mathrm{p},N}^{\mathrm{a}} + \exp(-2\gamma_i\Delta\varepsilon_{\mathrm{p}}^{\mathrm{a}})\chi_{i,N}^{\mathrm{m}} \tag{A.12}$$

which is also valid for $\gamma_k = 0$.

Since the constraint on imposed stresses must be fulfilled, Eq. (3) becomes:

$$\sum_{i=1}^{\mathrm{n}} \chi_{i,N}^{\mathrm{m}} = \sigma_{\mathrm{m}} \tag{A.13}$$

Note that Eq. (A.13) represents a hyperplane in the space $(\chi_1^{\mathrm{m}},\ldots,\chi_n^{\mathrm{m}})$, where n is the total number of back-stresses. At cycle N, the point $(\chi_{1,N}^{\mathrm{m}},\ldots,\chi_{n,N}^{\mathrm{m}})$ must belong to that hyperplane. The evolution law in Eq. (A.12) can be divided into two steps, as depicted in Fig. A.19:

$$\begin{aligned}
&\chi_{i,N}^{\mathrm{m}} \longrightarrow \exp(-2\gamma_i\Delta\varepsilon_{\mathrm{p}}^{\mathrm{a}})\chi_{i,N}^{\mathrm{m}} \longrightarrow \\
&\quad 2C_i\exp(-\gamma_i\Delta\varepsilon_{\mathrm{p}}^{\mathrm{a}})\Delta\varepsilon_{\mathrm{p},N}^{\mathrm{s}} + \exp(-2\gamma_i\Delta\varepsilon_{\mathrm{p}}^{\mathrm{a}})\chi_{i,N}^{\mathrm{m}} = \chi_{i,N+1}^{\mathrm{m}}
\end{aligned} \tag{A.14}$$

After the first step Eq. (A.14), the point $(\exp(-2\gamma_1\Delta\varepsilon_{\mathrm{p}}^{\mathrm{a}})\chi_{1,N}^{\mathrm{m}},\ldots,\exp(-2\gamma_n\Delta\varepsilon_{\mathrm{p}}^{\mathrm{a}})\chi_{n,N}^{\mathrm{m}})$ in general does not belong to the hyperplane of Eq. (A.13). In the second step of Eq. (A.14), $\Delta\varepsilon_{\mathrm{p},N}^{\mathrm{s}}$ restores the hyperplane constraint. Being $\Delta\varepsilon_{\mathrm{p},N}^{\mathrm{s}}$ the same for every χ_i^{m}, it does so through a translation along a line defined by the vector $(2C_1\exp(-\gamma_1\Delta\varepsilon_{\mathrm{p}}^{\mathrm{a}}),\ldots,2C_n\exp(-\gamma_n\Delta\varepsilon_{\mathrm{p}}^{\mathrm{a}}))$, which meets the hyperplane at a unique point. Thus, for each cycle there is a unique value of $\Delta\varepsilon_{\mathrm{p},N}^{\mathrm{s}}$ which ensures the fulfilment of the imposed stress constraints.

Eq. (A.12) is a first-order linear difference equation, having a characteristic root $\lambda = \exp(-2\gamma_i\Delta\varepsilon_{\mathrm{p}}^{\mathrm{a}}) < 1$. $\Delta\varepsilon_{\mathrm{p},N}^{\mathrm{s}}$ constitutes an external input which generates the forced response of Eq. (A.12). Since $\Delta\varepsilon_{\mathrm{p},N}^{\mathrm{s}} = B\exp(-G\Delta\varepsilon_{\mathrm{p}}^{\mathrm{a}}N)$, the latter will have the general form:

$$\chi_{i,N}^{\mathrm{m,forced}} = F_i\exp(-G\Delta\varepsilon_{\mathrm{p}}^{\mathrm{a}}N) \tag{A.15}$$

where $F_i \neq 0$.

Eqs. (A.10) and (A.15) are substituted in Eq. (A.12) in order to find the value of F_i, obtaining the following

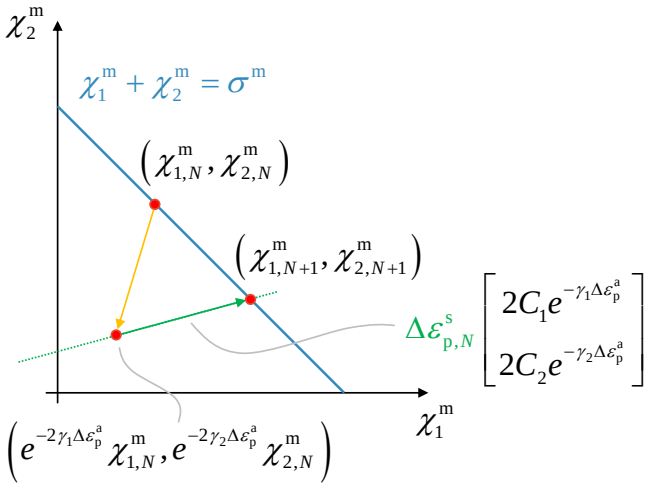

Figure A.19: Representative example of the evolution law Eq. (A.12), involving only two backstress components for clarity purposes.

result:

$$F_i = \frac{2C_i B}{\exp((\gamma_i - G)\Delta\varepsilon_{\mathrm{p}}^{\mathrm{a}}) - \exp(-\gamma_i \Delta\varepsilon_{\mathrm{p}}^{\mathrm{a}})} \tag{A.16}$$

Note that F_i cannot be null unless C_i or B are zero as well. When $\gamma_k = 0$, Eq. (A.16) becomes:

$$F_k = -\frac{2C_k B}{1 - \exp(-G\Delta\varepsilon_{\mathrm{p}}^{\mathrm{a}})} \tag{A.17}$$

The solution of Eq. (A.12) will be the superposition of the forced response from Eq. (A.15) with its free evolution, expressed by:

$$\begin{aligned} \chi_{i,N}^{\mathrm{m,free}} &= \theta_i \exp(-2\gamma_i \Delta\varepsilon_{\mathrm{p}}^{\mathrm{a}} N) \\ \chi_{i,N}^{\mathrm{m}} &= \chi_{i,N}^{\mathrm{m,free}} + \chi_{i,N}^{\mathrm{m,forced}} = \theta_i \exp(-2\gamma_i \Delta\varepsilon_{\mathrm{p}}^{\mathrm{a}} N) + F_i \exp(-G\Delta\varepsilon_{\mathrm{p}}^{\mathrm{a}} N) \end{aligned} \tag{A.18}$$

where θ_i depends on the boundary conditions.

Substituting Eq. (A.18) in the constraint (A.13), it follows that:

$$\begin{aligned} \sigma_{\mathrm{m}} = &\sum_{i=1\ i\neq k}^{n} \theta_i \exp(-2\gamma_i \Delta\varepsilon_{\mathrm{p}}^{\mathrm{a}} N) + \sum_{i=1\ i\neq k}^{n} \frac{2C_i B}{\exp((\gamma_i - G)\Delta\varepsilon_{\mathrm{p}}^{\mathrm{a}}) - \exp(-\gamma_i \Delta\varepsilon_{\mathrm{p}}^{\mathrm{a}})} \exp(-G\Delta\varepsilon_{\mathrm{p}}^{\mathrm{a}} N) \\ &+\theta_k - \frac{2C_k B}{1 - \exp(G\Delta\varepsilon_{\mathrm{p}}^{\mathrm{a}})} \exp(-G\Delta\varepsilon_{\mathrm{p}}^{\mathrm{a}} N) \end{aligned} \tag{A.19}$$

Eq. (A.19) implies that:

- $\theta_k = \sigma_{\mathrm{m}}$, in fact all other terms tend to zero as $N \to \infty$, except for θ_k.
- $G < 2\gamma_i$ for all index $i \neq k$. If this is not true, then the forced responses, proportional to $\exp(-G\Delta\varepsilon_{\mathrm{p}}^{\mathrm{a}} N)$, would at some point be negligible with respect to the slower free evolutions, proportional to $\exp(-2\gamma_i \Delta\varepsilon_{\mathrm{p}}^{\mathrm{a}} N)$. In fact, if a backstress component (denoted with index h) satisfies $G > 2\gamma_h$, Eq. (A.19)is approximated by:

$$\theta_h \exp(-2\gamma_h \Delta\varepsilon_{\mathrm{p}}^{\mathrm{a}} N) + \theta_k = \sigma_{\mathrm{m}} \tag{A.20}$$

By substituting $\theta_k = \sigma_\mathrm{m}$:

$$\theta_h \exp(-2\gamma_h \Delta\varepsilon_\mathrm{p}^\mathrm{a} N) = 0 \tag{A.21}$$

which cannot be satisfied for all N.

Instead, if $G < 2\gamma_i$ for all indexes i, Eq. (A.19) is approximated by:

$$\sum_{i=1\ i\neq k}^{n} \frac{C_i}{\exp((\gamma_i - G)\Delta\varepsilon_\mathrm{p}^\mathrm{a}) - \exp(-\gamma_i \Delta\varepsilon_\mathrm{p}^\mathrm{a})} = \frac{C_k}{1 - \exp(G\Delta\varepsilon_\mathrm{p}^\mathrm{a})} \tag{A.22}$$

Keeping usual index j for the smallest $\gamma_i > 0$, the constraint on G becomes $0 < G < 2\gamma_j$. In that interval, the right hand side of Eq. (A.22) monotonically decreases from $+\infty$ to $C_k/(1 - \exp(2\gamma_j \Delta\varepsilon_\mathrm{p}^\mathrm{a}))$, while the left hand side monotonically increases from $\sum_{i\neq k} C_i/(2\sinh(\gamma_i \Delta\varepsilon_\mathrm{p}^\mathrm{a}))$ to $+\infty$. Eventually, for any parameter set, there always exists a unique G which satisfies Eq. (A.22) and therefore the stress constraints. Since G is available from an experimental test, Eq. (A.22) may be used to find γ_j, if it is not known:

$$\frac{C_j}{\exp((\gamma_j - G)\Delta\varepsilon_\mathrm{p}^\mathrm{a}) - \exp(-\gamma_j \Delta\varepsilon_\mathrm{p}^\mathrm{a})} = \frac{C_k}{1 - \exp(G\Delta\varepsilon_\mathrm{p}^\mathrm{a})} - \sum_{i=1\ i\neq j,k} \frac{C_i}{\exp((\gamma_j - G)\Delta\varepsilon_\mathrm{p}^\mathrm{a}) - \exp(-\gamma_j \Delta\varepsilon_\mathrm{p}^\mathrm{a})} \tag{A.23}$$

As long as the right hand side of Eq. (A.23) is positive (which is reasonably true given $\gamma_i \gg \gamma_j > G/2$), there always exists a unique solution for γ_j. Since a ratcheting test preferentially requires a fair number of cycles before the specimen failure, it is quite common to have $\gamma_i \Delta\varepsilon_\mathrm{p}^\mathrm{a} \ll 1$ for all i. Since $G < 2\gamma_i$ for all i, $G\Delta\varepsilon_\mathrm{p}^\mathrm{a} \ll 1$ too. In this case Eq. (A.22) can be approximated as follows:

$$\sum_{\mathrm{i}=1\ \mathrm{i}\neq\mathrm{k}} \frac{C_i}{2\gamma_i - G} = \frac{C_k}{G} \tag{A.24}$$

Since for a slightly non-linear backstress component it usually holds that $C_j/\gamma_j \gg C_i/\gamma_i$, a sound assumption might be:

$$\frac{C_j}{2\gamma_j - G} \gg \frac{C_i}{2\gamma_i - G} \quad \text{for all } i \neq j \tag{A.25}$$

The hypothesis of Eq. (A.25) should be verified after the identification of parameters. Eventually, Eq. (A.24) becomes:

$$G = \frac{2\gamma_j}{C_j/C_k + 1} \tag{A.26}$$

Assuming that G is experimentally available, Eq. (A.26) allows an estimation of γ_j:

$$\gamma_j = \frac{G}{2}\left(\frac{C_j}{C_k} + 1\right) \tag{A.27}$$

Eqs. (A.15)-(A.27) are founded on the hypothesis that $\Delta\varepsilon_{\mathrm{p},N}^\mathrm{s} = B\omega^N$ for $A \neq 0$ and $0 < \omega < 1$. Although no formal proof that $\Delta\varepsilon_{\mathrm{p},N}^\mathrm{s}$ must have this form is available yet, numerical simulations suggest that it should actually be the case. Since these results concern the rate of convergence to the stabilized value $\Delta\varepsilon_{\mathrm{p},N}^\mathrm{s} = 0$ and not the stabilized value itself, they require the isotropic hardening to stabilize with a dynamic that is quicker than G, otherwise the material behavior would be dominated by the isotropic part and not by Eq. (A.12). Moreover, as most times G turns out to represent a particularly slow dynamic (especially when $C_k \ll C_j$), its identification

requires a precise instrumentation and many ratcheting cycles, which can be difficult to obtain, due to specimen failure. Due to this, the approach proposed in Section 2.5 should be preferred.

Appendix B. Electronic supplementary material

A MATLAB Graphical User Interface which implements this procedure has been uploaded to a GitHub repository: `https://github.com/grossIt/ChaPaFi`
For the sake of reproducibility, the stabilized cycles and the ratcheting tests for aluminum and steel specimens are available therein.

The same code and test data can also be found in the online version of the paper as electronic supplementary material. The provided files are:

- `ChaPaFi_v1_0.mlapp` – application to be run with graphical interface.
- `Alu_StabilizedCycle_1.mat` – first stabilized cycle for the aluminum alloy 7075-T6.
- `Alu_StabilizedCycle_2.mat` – second stabilized cycle for the aluminum alloy 7075-T6.
- `Steel_StabilizedCycle_1.mat` – first stabilized cycle for the steel 42CrMo4+QT.
- `Steel_StabilizedCycle_2.mat` – second stabilized cycle for the steel 42CrMo4+QT.
- `Steel_RatchetingCycle.mat` – ratcheting data for the steel 42CrMo4+QT.

Acknowledgment

This work was partially supported by grant PRA_2022_65 from the University of Pisa.